Particulate Metal Chalcogenides for Photocatalytic Z-Scheme Overall Water Splitting

Shanshan Chen,[1] Chenyang Li,[1] Kazunari Domen,[2,3,*] and Fuxiang Zhang[4,*]

[1] School of Materials Science and Engineering & National Institute for Advanced Materials, Nankai University, 38 Tongyan Road, Tianjin 300350, China

[2] Research Initiative for Supra-Materials, Interdisciplinary Cluster for Cutting Edge Research, Shinshu University, 4-17-1 Wakasato, Nagano-shi, Nagano 380-8553, Japan

[3] Office of University Professors, The University of Tokyo, 2-11-16 Yayoi, Bunkyo-ku, Tokyo 113-8656, Japan

[4] State Key Laboratory of Catalysis, *i*ChEM, Dalian Institute of Chemical Physics, Chinese Academy of Sciences, Dalian National Laboratory for Clean Energy, 457 Zhongshan Road, Dalian 116023, China

*Correspondence:

domen@chemsys.t.u-tokyo.ac.jp (K.D.)

fxzhang@dicp.ac.cn (F.Z.)

SUMMARY

Inspired by natural photosynthesis, photocatalytic Z-scheme overall water splitting (OWS) provides a renewable and scalable way to generate solar fuel of green hydrogen. To construct such efficient systems, it is the prerequisite that the used photocatalysts should have the ability of solar light utilization in wide spectral region. Metal chalcogenides is one kind of such promising narrow band gap semiconductors with tunable band structure and prominent photoelectronic properties. However, it is challenging at present mainly due to the photocorrosion and sluggish charge transfer kinetics. To address these issues, this review is devoted to providing a comprehensive illustration on the recent progress in this field. Herein, based on the analysis of the basics of photocatalytic Z-scheme OWS systems and metal chalcogenides, series approaches to drive Z-scheme OWS together with various strategies to prohibit the photocorrosion and improve the charge carrier utilization are elaborated. Future prospects and challenges in constructing efficient Z-scheme OWS systems with particulate metal chalcogenides are also discussed.

KEYWORDS: hydrogen production, metal chalcogenides, overall water splitting, photocatalysis, Z-scheme

INTRODUCTION

As global fossil fuel shortages and related environmental contamination issues continue to increase, it is imperative to develop clean and renewable energy resources without emitting carbon dioxide. Solar energy is one such kind of abundant and sustainable energy source. Various approaches have been developed for solar energy utilization, in which solar-driven overall water splitting (OWS) is one of the most promising ways to produce "green hydrogen".[1–6] More importantly, the produced solar fuel of hydrogen can be further applied for the hydrogenation of carbon dioxide, contributing to the reduction of global carbon dioxide emission.[7–9] Herein, it is the key that the development of scalable and efficient solar OWS systems. Three main types of systems such as photovoltaic-assisted electrolysis, photoelectrochemical (PEC) cells and photocatalysis have been extensively investigated, among which photocatalysis has been considered as one of the most promising ways due to the simplicity and low operational cost.[2,10] However, the current solar-to-hydrogen (STH) energy conversion efficiency via photocatalysis is the lowest, most of which is on the order of 1% at ambient pressure, below the economical requirement of 5–10%.[6,11–13] Development of efficient particulate OWS photocatalysts is still the mainstream at present.[14,15]

Generally, there are two distinct ways for photocatalytic OWS systems called one- and two-step photo-excitation routes.[16,17] The H_2 evolution and

water oxidation reactions occur on a single semiconductor photocatalyst for the one-step photo-excitation systems, while those redox reactions are performed at two different photocatalysts in the two-step photo-excitation systems (also called Z-scheme systems). As far as thermodynamics is concerned, it requires the semiconductors for one-step approach should have conduction band minimum (CBM) and valence band maximum (VBM) levels straddling the potentials of those redox reactions, while the semiconductors used for two-step approach can only possess a more negative CBM than the potential of the H_2 evolution reaction or a more positive VBM than the O_2/H_2O potential level. Therefore, the two-step system alleviates the thermodynamic requirements and expands the selection of semiconductors, especially for those with narrow band gaps. Up until now, various types of narrow band gap semiconductors have been used for two-step photoexcited OWS systems, such as doped oxides, (oxy)nitrides, (oxy)sulfides, oxyhalides, dye-sensitized semiconductors.[17–22] And the state-of-the-art particulate photocatalytic Z-scheme OWS system can deliver an STH conversion efficiency of 1.2% at 331 K and 10 kPa without external bias by employing Ru/Cr_2O_3-loaded $SrTiO_3$:La,Rh (< 520 nm), $BiVO_4$:Mo (< 520 nm) and C as a H_2 evolution photocatalyst (HEP), an O_2 evolution photocatalyst (OEP) and an electron mediator, respectively.[23] However, the absorption edges of the semiconductors used in this system are still limited, rendering the theoretical STH efficiency to be lower than the targeted value of about 5–10%. Accordingly, exploration and development of

narrow band gap photocatalysts as well as their construction for efficient solar Z-scheme OWS is still the current main research theme.

Metal chalcogenides is one such kind of narrow band gap semiconductors, which is composed of at least one chalcogen anion (S^{2-}, Se^{2-} or Te^{2-}) and at least one electropositive element.[24,25] Besides the narrow bandgap, some other features of flexible band structure, bio-compatibility and facile synthesis make it be extensively investigated in the field of solar energy conversion, such as photovoltaics, PEC cells and photocatalysis.[26–28] Notely that metal chalcogenides can be used for high-efficient low-cost thin-film solar cells, such as $Cu(In,Ga)Se_2$ and CdTe, whose certified cell efficiency has been achieved as high as 23.4%, comparable to that of the crystalline silicon-based and perovskite solar cells.[29] Inspired by its excellent photoelectronic properties of metal chalcogenides, it is reasonably expected to use them as efficient photocatalysts in consideration of the shared similar photophysical processes, such as light absorption and charge separation, although some critical challenges including photocorrosion and sluggish charge transfer kinetics need to be confronted.

To date, considerable progress has been achieved recently by using metal chalcogenides for photocatalytic OWS, especially for the fabrication of effective Z-scheme systems.[30–32] It has already been demonstrated that visible-light-driven photocatalytic Z-scheme OWS can be realized by using metal

chalcogenides as HEPs, and the relationship between structure and performance has been illustrated accordingly.[30,33] What's more important, the apparent quantum yield (AQY) presently achieved is even comparable to that of other types of popularly investigated semiconductors, such as oxyhalogenide.[20,32] Several reviews have already been reported on the advances of metal chalcogenides for photocatalytic hydrogen production in the presence of sacrificial agents, that is to say, for the half-reaction of water splitting.[25,28,34,35] However, to the best of our knowledge, there is no review focusing on summarizing and analyzing its application in photocatalytic Z-scheme OWS. This paper is devoting to filling this gap to give an overview on the photocatalytic Z-scheme OWS based on metal chalcogenides. Meanwhile, basic properties of metal chalcogenides related to the photocatalytic process are introduced together with its synthetic methods. Moreover, its application to photocatalytic Z-scheme OWS in several distinct approaches is classified and illustrated, and the structure-performance relationship is analyzed and revealed to provide guidelines to fabricate more efficient systems. Finally, we describe future prospects and challenges in overcoming the key issues hindering the realization of efficient Z-scheme OWS with metal chalcogenides.

BASICS OF PHOTOCATALYTIC Z-SCHEME OWS

Since the discovery of the Honda-Fujishima effect, considerable progress

including photocatalytic materials and OWS systems has been made in this field.[14,36] As branded as a Holy Grail of chemistry, photocatalytic OWS is a promising scalable and economically feasible technology for the production of renewable solar fuels. It is a thermodynamically uphill chemical reaction with an associated increase in the Gibbs free energy ($\Delta G° = 237$ kJ mol^{-1}), by which solar energy can be captured and converted to chemical energy. It is noteworthy that besides the OWS reaction, the H_2 and O_2 evolution in the presence of sacrificial reagents (called as half reactions) have been extensively investigated to evaluate the potential of one photocatalyst and to insight its underlying key factors limiting H_2 and O_2 evolution. However, these reactions are generally downhill processes associated with decrease in the Gibbs free energy or with very low values, rendering the storage of solar energy ineffective or infeasible.[37] Therefore, in order to realize the storage and conversion of solar energy, achievement of photocatalytic OWS reaction is highly desirable.

As indicated in the above section, one- and two-step photo-excitation routes are commonly used for photocatalytic OWS.[17] For the one-step photo-excitation system, it is generally a single particulate photocatalyst composed of a light-harvesting semiconductor and one or more cocatalyst(s). Herein, the semiconductor is primarily responsible for the progression of photon absorption and the separation of charge carriers, while H_2 and O_2 evolution reactions occur mainly on the surface of cocatalyst(s). For the two-step photo-excitation system, it mainly consists of an HEP and an OEP. As described in Figure 1, H^+ was

reduced to H_2 by photogenerated electrons over the HEP, whereas H_2O was oxidized to O_2 by holes generated from the OEP. Then, the remained photoexcited holes in the HEP and electrons in the OEP recombined via an aqueous redox mediator (Figure 1A) or a solid-state electron mediator (Figure 1B) to complete the whole reaction cycle. More specifically, reductant oxidation and oxidant reduction reactions occurred on the HEP and OEP, respectively, in the case of Z-scheme system with an aqueous redox mediator. While for the latter case, electrons from the HEP and holes from the OEP would transfer to the solid-state electron mediator and recombine there. This kind of systems is inspired by natural photosynthesis in green plants, which was proposed in 1979 and experimentally demonstrated until 2001, where I^-/IO_3^- was used as an aqueous redox mediator.[38,39] To date, this kind of Z-scheme OWS systems has been fully developed, in which series aqueous redox couples based on the valence changes of $I^{(1-/0)}$, $I^{(1-/5+)}$, $Fe^{(2+/3+)}$, $Co^{(2+/3+)}$, $V^{(4+/5+)}$, $Mn^{(2+/3+)}$, and $Mo^{(5+/6+)}$ have been applied.[40–47] Among those reported systems, the highest efficient one has been demonstrated to be constructed by employing $[Fe(CN)_6]^{3-/4-}$ as a redox mediator, $Rh_yCr_{2-y}O_3$ loaded ZrO_2/TaON or $MgTa_2O_{6-x}N_y$/TaON as an HEP, and Ir-$FeCoO_x$/$BiVO_4$ as an OEP.[48] Herein, an AQE as high as 12.3% at 420 nm and an STH value of 0.6% were reported for photocatalytic OWS.

For the case of the all-solid-state Z-scheme system, it was firstly demonstrated by Tada et al. in 2006, where Au nanoparticles were used as the recombination channel of the electrons from TiO_2 and holes from CdS.[49] Then,

this mechanism was applied to drive OWS reaction based on the combination of Ru/$SrTiO_3$:Rh and $BiVO_4$ photocatalysts, in which a type of reversible $Rh^{3+/4+}$-redox species on the HEP surface played a pivotal role in the electron-hole recombination at the interparticle.[50] Notably, our group further upgraded this system by introducing a conductive layer, which served as an electron mediator and a physical bridge to link HEP and OEP particles.[51,52] The fabricated system was in a sheet form, which could reduce the interfacial resistance between the conductive layer and photocatalysts, leading to the promoted electron-hole recombination at the mediator. Moreover, the developed photocatalyst sheet could be manufactured in large-scale by a simple printing technique with ink containing a colloidal electron mediator, HEP and OEP particles. In addition, the produced sheet photocatalyst can be easily collected and replaced during the reaction, both of which are beneficial for the practical application.[53] Up until now, various solid-state electrical conductors, such as Ir, Ag, Au, Rh, Ni, Pt, reduced graphene oxide (RGO), indium tin oxide (ITO) and C, have been identified as electron mediators for Z-scheme OWS systems, where the STH value can be achieved even over 1%, demonstrating the high potential in efficient solar OWS.[23,51,54–58]

Compared with the one-step photo-excitation system, the Z-scheme system shows several advantages in the following aspects. The first one is that it can relax the thermodynamic requirements of the OWS reaction, making more narrow band gap semiconductors possible be used. As mentioned above,

various types of particulate photocatalysts including doped oxides, (oxy)nitrides, (oxy)sulfides, oxyhalides, have been intensively investigated for Z-scheme OWS.[17–21] More specifically, semiconductors with a more negative CBM than the potential of the H_2 evolution reaction or a more positive VBM than the O_2 evolution reaction can be used, leading to a large driving force in the Z-scheme system. For instance, most metal chalcogenides can not evolve oxygen from water thermodynamically due to their negative VBM compared to the O_2/H_2O potential level. However, they can be used as HEPs in the Z-scheme OWS systems, which will be detailly illustrated in the subsequent sections.[31] In addition, it is also possible to collect the evolved H_2 and O_2 gases separately by spatial division of the H_2 and O_2 catalytic sites in a Z-scheme system.[41]

However, besides the common side reactions of O_2 reduction reaction (ORR) and H_2 oxidation reaction (HOR) in one-step photoexcitation systems, the Z-scheme OWS system also suffers from backward electron transfer reactions (see Figure 1A) due to the additional elementary procedures involved with redox couples.[59] For all-solid-state Z-scheme systems, instead of aqueous redox couples, conductive materials are used for the recombination of photoexcited electrons from OEPs and holes from HEPs (see Figure 1B). Herein, side reactions of backward electron transfer routes containing redox mediators can be avoided. Although the Z-scheme system has various advantages over the one-step photo-excitation system, the theoretical STH conversion efficiency of the former (i.e., AQY of unity) will be half of that of the

latter if the same photocatalysts or them with the same light absorption efficiency are used. Of course, the absorption edge of photocatalysts used for Z-scheme systems can be greatly extended in reality. A comprehensive comparison of these two distinct systems is therefore summarized and given in Table 1.

Table 1. Comparison of one- and two-step photoexcitation OWS systems

Items \ Types	One-step photoexcitation system	Two-step photoexcitation system	
		Aqueous redox mediator	Solid electron mediator
Number of the essential light-harvesting semiconductors	1	2	2
Number of photons needed for each cycle	4	8	8
Theoretical maximum STH conversion efficiency	100%	50%	50%
In-situ separation of the evolved H_2 and O_2 gases	Impossible	Possible	Possible
Driving force of reactions	Small	Large	Large
System complexity	Moderate	Complicated	Complicated
Band gap requirement of the light-harvesting semiconductors	Straddling the H^+/H_2 and O_2/H_2O redox potentials	HEP: the CBM is more negative than the H^+/H_2 potential; OEP: the VBM is more positive than the O_2/H_2O potential	
Backward/side reactions	ORR, HOR	ORR, HOR, and redox mediator-involved backward electron transfer reactions	ORR, HOR

OWS, overall water splitting; ORR, O_2 reduction reaction; HOR, H_2 oxidation reaction; STH, solar to hydrogen; VBM, valence band maximum; CBM, conduction band minimum; HEP, H_2 evolution photocatalyst; OEP, O_2 evolution photocatalyst.

BASICS OF METAL CHALCOGENIDES FOR PHOTOCATALYTIC Z-SCHEME OWS

Metal chalcogenides is one kind of semiconductors composed of at least one chalcogen anion (S^{2-}, Se^{2-} or Te^{2-}) and one electropositive element. Due to the excellent properties in photoelectricity and flexible band structure, it has been widely used as light harvesters for solar energy conversion including photocatalysis.[26–28,60] Some momentous photocatalytic applications of water splitting, CO_2 reduction, pollutants degradation, and fine chemical synthesis have been extensively exploited.[61–67] For the case of photocatalytic OWS, most of them were applied as HEPs in Z-scheme approaches, whose structural and photophysical properties needed to be finely modulated to function their maximum performances.

As for the property of band structure, it can be seen from Figure 2A that the constituent cations in the applied metal chalcogenides are mostly the metals with d^{10} configuration, such as Cu, Zn, Ga, Ag, Cd, and In.[65,68] Therefore, the CBM is mainly affected by the orbitals of the metal, whereas the VBM is mainly derived from the p-orbitals of chalcogens (S, Se, Te) or its hybrid with d-orbitals of the constituent transition metal (Figure 2B). Note that the atomic orbital energies of chalcogenide p (S, Se, Te) are close to each other but not to that of O 2p, making it distinguished from metal oxides. Combining with the aforementioned analysis on the orbitals-constituent band structure, it can be concluded that the CBM is negative enough for H_2 evolution reaction and narrow band gaps can be easily obtained by tuning the composed elements. According to the number of the constituent elements, metal chalcogenides is

generally classified to binary and multinary chalcogenides, such as CdS, ZnS and $CuGaSe_2$ (Figure 2B). In addition, based on the similar crystal structure, some metal chalcogenides can also form solid solutions with various compositions.[37] It is the diversity of the consisted elements with different proportions that endows the flexible features of metal chalcogenides in band and crystal structures. Take zinc chalcogenides as an example, the absorption edge is changed from 335 nm (3.7 eV) to 480 nm (2.6 eV) and then to 540 nm (2.3 eV), when chalcogens of S, Se, and Te are used, respectively (Figure 2C). Under this circumstance, the energy levels of the CBM are similar, while those of the VBM gradually decrease, leading to the decrease in the driving force of the hole-involved oxidation reaction and the increased difficulty in achieving Z-scheme process. ZnS (or ZnSe) can be further combined with silver indium sulfide or copper gallium sulfide (or corresponding selenide) to form a series of solid solutions, whose absorption edges and semiconductor characteristics (p- or n-type) can be finely tuned by the compositions.[31,43,69] Therefore, those features of adjustable CBM position, flexible modulation of band structure and tunable semiconductor characteristics make metal chalcogenides over most other types of visible-light responsive semiconductors to be appealing HEPs for photocatalytic Z-scheme OWS.

Another advantage of metal chalcogenides is that it can be prepared with high crystallinity and low defect density, both of which are beneficial to the enhanced charge separation and photo-stability.[70] Various synthesis methods

have been developed to obtain particulate metal chalcogenides, which contain solid-state reaction (SSR), hydrothermal, hot injection, and sol-gel methods, etc.[71–74] Among them, the SSR and hydrothermal routes have been the most popularly used due to their simplicity, scalability and the preponderance in easy control of crystallinity, particle size and morphology. Recently, flux-assisted SSR method has been developed, by which single crystal of metal chalcogenides can be synthesized and the preparation temperature can be remarkably reduced compared to that in the traditional SSR method, leading to enhanced charge separation.[75,76] It is believed metal chalcogenides can be endowed with promoted properties by rationally applying the advanced preparation methods.

When metal chalcogenides is applied for photocatalytic OWS, one big challenge needed to be conquered is the prohibition of the severe self-photocorrosion caused by the photogenerated holes to decompose itself, rendering holes to participate in water oxidation or hole-involved Z-scheme process. To mitigate this issue, continuous efforts have been made to focus on the construction of efficient water oxidation catalytic sites including the incorporation of oxidation cocatalysts and metal dopants in the one-step photoexcited OWS approach.[77] For example, CdS possesses excellent charge transfer properties, a band gap of approximately 2.4 eV and suitable band alignment for the thermodynamic necessity for OWS reaction. By rational loading of Pt and PdS nanoparticles as reduction and oxidation cocatalysts, respectively, an extremely high AQY of 93% at 420 nm was achieved over CdS

for stable sacrificial H_2 evolution.[72,78] Simultaneous H_2 and O_2 evolution was also reported to be observed on CdS nanorods by co-modified with Pt reduction cocatalyst and Ru(tpy)(bpy)Cl_2-based oxidation catalysts in pure water for OWS.[79] However, the obtained H_2/O_2 molar ratio still deviated from the stoichiometric value of 2, due to the oxidation of S^{2-} ions and the cysteine ligands by holes. Recently, accelerated reaction kinetics stemming from Ag dopants on boosting O_2 evolution reaction has been demonstrated over Ag doped $ZnIn_2S_4$, leading to stoichiometric H_2 and O_2 evolution in pure water under visible light irradiation.[77] In addition, one-step photoexcited OWS over series metal sulfides was reported by rapid separation of the evolved O_2 from H_2 via the artificial gill to prohibit the reversion reaction of H_2O formation, which could provide useful guidance in the design and construction of artificial photosynthesis systems.[80,81]

Compared with the case of one-step photoexcited OWS system, it is easy to prohibit photocorrosion in a Z-scheme OWS system in which metal chalcogenides is used as an HEP.[82] It is because the oxidation of the reduced couple is easier to occur from the view point of thermodynamics than water oxidation reaction, due to the relatively low redox potential of the former reaction. Moreover, owing to the relaxation of the thermodynamic requirements of the Z-scheme OWS systems, various metal chalcogenides without water oxidation ability but capable of evolving H_2 from an aqueous solution containing appropriate sacrificial reagents can be applied. The timeline of the key

developments in photocatalytic Z-scheme OWS using particulate metal chalcogenides is summarized and given in Figure 3. Since the first demonstration of Z-scheme OWS system employing CdS as an HEP was reported in 2014, series photocatalytic Z-scheme OWS systems with different electron mediators and configurations have been developed.[30,43,83,84] Besides metal sulfides, metal selenides was also validated to be feasible to act as an HEP for Z-scheme OWS in 2019, and subsequently systems with different solid-state electron mediators were correspondingly reported.[31,85] Among those developed Z-scheme OWS systems, an enhanced AQY of 1.5% at 420 nm had been achieved, which was realized by constructing an appropriate p-n junction ($(CdS/(ZnSe)_{0.5}(CuGa_{2.5}Se_{4.25})_{0.5})$ to promote the charge separation of the selenide semiconductor.[32] To our knowledge, this should be the highest value among the reported photocatalytic Z-scheme OWS systems with metal chalcogenide HEPs so far. A detailed analysis on metal chalcogenides for photocatalytic Z-scheme OWS will be given in the following section.

PROGRESS OF Z-SCHEME OWS WITH METAL CHALCOGENIDE PHOTOCATALYSTS

Since the original model of the Z-scheme system using particulate photocatalysts was firstly proposed in 1979, it was not successfully demonstrated in experiment until more than two decades afterwards.[39] In 2001,

the first Z-scheme OWS system was realized by Abe et al., in which TiO_2 photocatalysts with phases of anatase and rutile were used as an HEP and an OEP, respectively.[38] Considering the applied TiO_2 photocatalysts only function under ultraviolet light, to utilize wider wavelength range of solar spectrum, extensive effort has been made after that to apply visible light responsive photocatalysts, especially for those with narrow band gaps. In late 2001, the first visible-light-driven Z-scheme OWS system was developed, where $Pt/SrTiO_3$:Cr,Ta, PtO_x/WO_3 and IO_3^-/I^- were used as an HEP, an OEP and a redox mediator, respectively.[87] Since then, various types of narrow band gap semiconductors have been intensively investigated.[17–21] In 2014, the first Z-scheme OWS process with CdS acting as an HEP was demonstrated by Li et al. (see the timeline in Figure 3).[83] It means the research history of Z-scheme OWS with metal chalcogenide photocatalysts is only about 9 years until now. However, its development progress is very remarkable. A summary of representative systems for Z-scheme OWS with particulate metal chalcogenides was given in Table 2. Series metal sulfides and metal selenides with absorption edges ranging from 540 to 860 nm were applied, and the highest AQY of 1.5% at 420 nm had been achieved.[30,32] According to the difference in mediators and system configurations, three types are classified, which are aqueous redox mediator in a powder suspension system, solid-state electron mediator in a powder suspension system, and solid-state electron mediator in a sheet system. To give deep illustration of the design guidelines

and the corresponding system assembly for those types, detailed description was summarized and provided in the following sub-sections.

Table 2. Typical photocatalytic Z-scheme OWS systems employing particulate metal chalcogenide HEPs

Entry	HEP (available wavelength)	OEP(e) (available wavelength)	Mediator (V vs. NHE)	Reactant solution	Efficiency	Refs
Aqueous redox mediator in a powder suspension system						
1	Ru_2S_3/CdS (< 540 nm)	Photosystem II (400–520 and 600–700 nm)	$Fe(CN)_6^{3-/4-}$ (0.358)	H_2O (50 mM sodium phosphates, 15 mM NaCl, pH = 6.0)	No data	83
2	Pt/CdS (< 540 nm)	CoO_x/TaON photoanode (< 520 nm)	$Fe(CN)_6^{3-/4-}$ (0.358)	H_2O (0.1 M borate, pH = 8.0)	No data	88
3	Pt/$Zn_{0.75}Cd_{0.25}Se$ (< 750 nm)	CoO_x/TaON photoanode (< 520 nm)	$Fe(CN)_6^{3-/4-}$ (0.358)	H_2O (0.3 M borate, pH = 9.0)	AQY: 0.0082% at 400 nm	89
4	Ru/$(CuGa)_{0.8}Zn_{0.4}S_2$ (< 560 nm)	$BiVO_4$ (< 520 nm)	$[Co(terpy)_3]^{3+/2+}$ (no data)	H_2O	STH value: 0.0025%	43
5	MoS_2/CdS (< 540 nm)	Co_3O_4/$BiVO_4$ (< 520 nm)	$[Co(bpy)_3]^{3+/2+}$ (0.30)	H_2O	AQY: 1.04% at 420 nm	90
6	NiS/CdS (< 540 nm)	PtO_x/WO_3 (< 465 nm)	I_3^-/I^- (0.536)	H_2O (H_2SO_4, pH = 4.0)	No data	84
Solid-state electron mediator in a powder suspension system						
7	• Pt/$CuGaS_2$ (< 540 nm) • Pt/Cu_2ZnGeS_4 (< 540 nm) • Pt/$CuInS_2$ (< 770 nm) • Pt/Cu_2ZnSnS_4 (< 860 nm)	TiO_2 (rutile, < 400 nm)	RGO	H_2O	STH value: 0.023% (in the case of Pt/$CuGaS_2$)	30
8	Pt/$(CuGa)_{0.5}ZnS_2$ (< 560 nm)	CoO_x/$BiVO_4$ (< 520 nm)	RGO	H_2O	AQY: 0.80% at 440 nm, STH value: 0.024%	75
9	Pt/$ZnIn_2S_4$ (< 570 nm)	CoO_x/Bi_2MoO_6 (< 460 nm)	RGO	H_2O	No data	91
10	Pt/ $(ZnSe)_{0.5}(CuGa_2Se_{3.5})_{0.5}$ (< 690 nm)	CoO_x/$BiVO_4$ (< 520 nm)	RGO	H_2O	No data	85
11	CdS (< 540 nm)	$BiVO_4$ (< 520 nm)	CDs	H_2O	H_2O	92
12	PtS/$ZnIn_2S_4$ (< 570 nm)	MnO_2/WO_3 (< 475 nm)	None	H_2O	AQY: 0.50% at 420 nm	93
Solid-state electron mediator in a sheet system						
13	Pt/Cr_2O_3/ZCGSe (< 690 nm)	CoO_x/$BiVO_4$ (< 520 nm)	Au	H_2O	AQY: 0.54% at 420 nm	31
14	Pt/TiO_2-CdS-ZCGSe (< 725 nm)	$BiVO_4$:Mo (< 520 nm)	Au	H_2O	AQY: 1.5% at 420 nm	32

HEP, H_2 evolution photocatalyst; OEP(e), O_2 evolution photo(electro)catalyst; NHE, normal hydrogen electrode; Refs, references; STH, solar to hydrogen; AQY, apparent quantum yield; RGO, reduced graphene oxide; CDs, carbon dots; ZCGSe, $(ZnSe)_{0.5}(CuGa_{2.5}Se_{4.25})_{0.5}$; $[Co(terpy)_3]^{3+/2+}$, (terpy = 2,2':6',2"-terpyridine); $[Co(bpy)_3]^{3+/2+}$, (bpy = 2,2'-bipyridine); OWS, overall water splitting.

Aqueous redox mediator in a powder suspension system

In this approach, particulate metal chalcogenides is used as an HEP suspended in the reaction solution, and an aqueous redox mediator is introduced to recombine holes from the HEP and electrons from an O_2 evolution part. The part of O_2 evolution can be constructed in various ways, such as photocatalysis, photoelectrocatalysis and biocatalysis, whose main function is to oxidize water to produce O_2 gas and reduce the oxidant from the HEP (Figure 1A). Herein, the selection of the aqueous redox mediator is very important for the Z-scheme process. It requires the occurrence of the reductant oxidation reaction should be preferred to the photocorrosion reaction over the metal chalcogenide HEP, so that the electron cycle between the HEP and the O_2 evolution part can be ensured. Among the various reported redox mediators, $[Fe(CN)_6]^{3-}/[Fe(CN)_6]^{4-}$, I_3^-/I^- and cobalt-based redox couples are mainly studied (Table 2).[43,83,84] To give a detailed elucidation of the recent key progress in this system, those aforementioned types of redox mediators are mainly focused and illustrated in the following parts.

Recently, $[Fe(CN)_6]^{3-}/[Fe(CN)_6]^{4-}$ shuttle ions have been popularly applied for Z-scheme OWS with metal chalcogenide HEPs. It can work at much milder pH environment than the case of Fe^{3+}/Fe^{2+} couple ($[Fe(CN)_6]^{3-}/[Fe(CN)_6]^{4-}$: pH 6–7; Fe^{3+}/Fe^{2+}: pH 2–3), and can be cycled by accepting/donating only one

electron instead of multiple electrons like the redox mediator of IO_3^-/I^- (6 electrons).[40,42,94] It is not favorable for Fe^{3+}/Fe^{2+} shuttle ions to assemble a Z-scheme system with a metal chalcogenide photocatalyst, because iron ions will react with metal chalcogenides to form iron chalcogenides, and metal chalcogenide photocatalysts are not stable at low pH in which the redox couple of Fe^{3+}/Fe^{2+} can be used.[84] Accordingly, those advantages of $[Fe(CN)_6]^{3-}/[Fe(CN)_6]^{4-}$ redox couple render it more favorable to apply metal chalcogenides for Z-scheme OWS. The first successful example is one such system with $[Fe(CN)_6]^{3-}/[Fe(CN)_6]^{4-}$ couple as a redox mediator, in which Ru_2S_3/CdS is used for H_2 evolution and photosystem II (PSII) membrane fragments function as a water oxidation catalyst (Figure 4).[83] Although the obtained OWS efficiency was not high at that time, this work opened a new avenue to achieve a Z-scheme OWS process via a bio-hybrid approach and inaugurated a new application of metal chalcogenide photocatalysts.[95,96]

Based on the aqueous redox mediator of $[Fe(CN)_6]^{3-}/[Fe(CN)_6]^{4-}$, Abe et al. further developed a photocatalysis-photoelectrocatalysis coupled Z-scheme system, where Pt/CdS was used as an HEP, and CoO_x/TaON photoanode was applied for water oxidation reaction (Figure 5A).[88] This work enriched the application ways of Z-scheme OWS with metal sulfides as an HEP. Furthermore, metal selenide of $Zn_{0.75}Cd_{0.25}Se$ was also successfully demonstrated to be feasible in constructing such kind of system for OWS, implying the high application potential of metal chalcogenides in this approach.[89] However, the

aforementioned O_2 evolution parts of PSII and CoO_x/TaON photoanode are belong to categories of natural photosynthesis and photoelectrocatalysis, respectively. Development of Z-scheme OWS systems fully composed of photocatalysts will be more desirable in consideration of scalability, stability and cost. Recently, our group has developed series $[Fe(CN)_6]^{3-}$/$[Fe(CN)_6]^{4-}$ mediated Z-scheme OWS systems with $MgTa_2O_{6-x}N_y$/TaON and $BiVO_4$ as an HEP and an OEP, respectively.[48,94] An AQY of 12.3% at 420 nm could be achieved over this system, which is the highest value among the suspended particulate photocatalytic OWS systems using inorganic semiconductors.[48] It is believed metal chalcogenides is also promising to be assembled to such photocatalytic Z-scheme system for efficient OWS.

Besides $[Fe(CN)_6]^{3-}$/$[Fe(CN)_6]^{4-}$ shuttle ions, cobalt-based redox couples, including $[Co(bpy)_3]^{2+/3+}$ (bpy = 2,2'-bipyridine), $[Co(phen)_3]^{2+/3+}$ (phen = 1,10-phenanthroline) and $[Co(terpy)_3]^{2+/3+}$ (terpy = 2,2':6',2"-terpyridine) complexes were also reported to be feasible in bridging an HEP of metal sulfides and an OEP of $BiVO_4$ to achieve an effective Z-scheme OWS process (Table 2).[43,90] For example, Kudo et al. reported when $[Co(terpy)_3]^{2+/3+}$ ions were employed as redox couple, Ru-loaded $(CuGa)_{0.8}Zn_{0.4}S_2$ and $BiVO_4$ functioned as an HEP and an OEP, respectively, a Z-scheme OWS system could be assembled, with an STH value of approximately 0.0025%. Herein, cobalt-based redox couple shares similar features with that of $[Fe(CN)_6]^{3-}$/$[Fe(CN)_6]^{4-}$ shuttle ions, both of which can be cycled with only one electron, possess redox potentials of

approximately 0.3 V vs. NHE and can be operated under near-neutral conditions (Table 2). In addition, very recently I_3^-/I^- redox couple has been identified to be feasible to mediate a photocatalytic Z-scheme OWS system, where NiS/CdS and PtO_x/WO_3 are used as an HEP and an OEP, respectively.[84] This result further expands the types of the applied redox mediators, and provides us more references to construct effective Z-scheme processes with metal chalcogenides.

Although several aqueous redox couples have been demonstrated to be feasible for metal chalcogenide photocatalysts used in Z-scheme OWS systems, the successful reported examples are still limited, primarily due to the insufficient oxidation rate of the reductant on the metal chalcogenide photocatalysts. In other words, photocorrosion and/or oxidative deactivation (i.e., formation of inactive oxide layers) occurs competitively if the oxidation rate of the reductant on the metal chalcogenide photocatalysts is insufficient, even though the VBM of the metal chalcogenides is thermodynamically sufficient for the reductant oxidation reaction. Therefore, it is necessary to develop effective strategies to facilitate H_2 evolution and reductant oxidation reactions while inhibit the self-oxidative deactivation process and the backward electron-transfer reaction over metal chalcogenide photocatalysts. To address those issues, besides the selection of proper redox mediators, surface modification of metal chalcogenide photocatalysts is another way. For instance, Abe et al. developed a versatile strategy involving the formation of a thin protective and

catalytic complex layer to stabilize metal sulfides, including CdS, $ZnIn_2S_4$ and $CdIn_2S_4$, as HEPs for Z-scheme OWS mediated by $[Fe(CN)_6]^{3-}/[Fe(CN)_6]^{4-}$ redox couple.[88,97] Specifically, in the initial period of the photocatalytic reaction, $K_2[CdFe(CN)_6]$ was spontaneously formed and covered on the Pt/CdS photocatalyst surface. The formed $K_2[CdFe(CN)_6]$ could efficiently consume photogenerated holes in the Pt/CdS and oxidize $[Fe(CN)_6]^{4-}$ to $[Fe(CN)_6]^{3-}$, leading to stable H_2 evolution (Figure 5B). It means the $K_2[CdFe(CN)_6]$ species acts as both a hole-transport agent and an effective surface modifier, which mitigates the photocorrosion of Pt/CdS during the photocatalytic reaction.[88] Similar cyanoferrates (i.e., $K_xM[Fe(CN)_6]_y$, M = Zn, In) were further developed to ensure stable and efficient H_2 evolution based on metal sulfide or metal selenide photocatalysts.[89,97] In summary, both surface modification of metal chalcogenide photocatalysts and aqueous redox mediators need to be carefully modulated to realize an effective reductant oxidation reaction during the Z-scheme OWS process.

Solid-state electron mediator in a powder suspension system

In this approach, different from the suspended system with an aqueous redox mediator, the recombination of holes from metal chalcogenide photocatalysts for H_2 evolution and electrons from OEPs is carried out either via a solid-state electron mediator or via physical contact (Figure 1B). Therefore,

some backward electron transfer reactions involving aqueous redox mediators can be avoided. However, it additionally suffers from the recombination of electrons from the metal chalcogenide photocatalysts and holes from the OEP, if a rectification function is not induced.[17] The charge transfer direction between the HEP/(electron mediator)/OEP interfaces can be rectified by regulating the band bending in those space-charge layers.[98] Therefore, some related properties, such as the band structure of the introduced HEP and OEP, and the work function of the solid-state electron mediator, need to be carefully examined to achieve the desired Z-scheme process.[23,99]

The first example of the solid-state Z-scheme OWS system was reported by Kudo et al. In this system, various metal sulfides were applied as HEPs, and RGO and TiO_2 with rutile phase were used as an electron mediator and an OEP, respectively (Figure 3).[30] It was found that metal sulfide photocatalysts with a p-type semiconductor character, such as $CuGaS_2$, $CuInS_2$, Cu_2ZnGeS_2, and Cu_2ZnSnS_2, were feasible to achieve a Z-scheme process, when they were coupled with an n-type TiO_2 bridged by the RGO (Table 2). While for metal sulfides with n-type semiconductor properties, Z-scheme process did not proceed. Considering TiO_2 can only absorb ultra-violet light, a visible-light-responsive $CoO_x/BiVO_4$ was further introduced to replace it as an OEP. In this case, Z-scheme OWS could be driven by visible light.[33] As shown the schematic diagram in Figures 6A and B, H_2 and O_2 evolution reactions occur on the surfaces of metal sulfide and $CoO_x/BiVO_4$ photocatalysts, respectively. The

remained holes in the metal sulfide photocatalyst and electrons in $CoO_x/BiVO_4$ will recombine via the RGO "channel" to complete the whole Z-scheme cycle.

The working principle of such system is similar to that for a p-n PEC cell (Figure 6C), in which a metal sulfide photocathode and a $CoO_x/BiVO_4$ photoanode are connected by an RGO "wire", and OWS is driven on such miniature device without external bias.[33,100] Detailed analysis showed that one key prerequisite to achieve such process was that the photoanode and the metal sulfide photocathode should generate photocurrent within the same potential window, which meant that the onset potential of the photocathode should be higher than that of the photoanode, leading to an overlapped range between the potentials for the cathodic and anodic photocurrent (Figure 6D). In such circumstance, the photogenerated electrons in the photoanode can migrate to the metal sulfide photocathode through the RGO without the assistance of external bias. Based on those understandings, p-type metal selenide of $(ZnSe)_{0.5}(CuGa_2Se_{3.5})_{0.5}$ (a solid solution of ZnSe and $CuGa_2Se_{3.5}$) was also successfully demonstrated to be feasible as an HEP to construct an effective Z-scheme OWS system with an OEP of $CoO_x/BiVO_4$ mediated by the RGO, suggesting the universality of such type of systems for metal chalcogenide photocatalysts.[85]

As for the solid-state electron mediator, besides RGO it was demonstrated that carbon dots were also effective in constructing Z-scheme OWS systems

with metal chalcogenide photocatalysts. For example, a Z-scheme OWS process was reported to be achieved by employing CdS and $BiVO_4$ as an HEP and an OEP, respectively.[92] Although the aforementioned two carbon-based conductors (RGO and carbon dots) were identified to be feasible as the solid-state electron mediators for Z-scheme OWS systems involving metal chalcogenide photocatalysts, the type and number of the identified electron mediators were still very limited. Some other electrical conductors, such as Ir and Ag, had already been verified to be effective solid-state electron mediators when they were cooperated with photocatalysts other than metal chalcogenides to construct powder-suspended Z-scheme OWS systems.[56,57] It is believed these electron mediators are also possible to be applied for cases with metal chalcogenide photocatalysts. In addition, photocatalytic Z-scheme OWS process can even occur without the addition of any electron mediators.[18,50] In this circumstance, interparticle electron transfer occurs directly between the HEP and OEP particles, which are in physical contact with each other. This kind of systems can avoid side reactions and light-shielding involved with the solid-state electron mediator.[82] For example, Li et al. reported that PtS-$ZnIn_2S_4$ HEP and MnO_2-WO_3 OEP could be combined by a self-assembly method, and the fabricated PtS-$ZnIn_2S_4$/MnO_2-WO_3 nanocomposites could split pure water via a Z-scheme mechanism to produce H_2 and O_2 under visible light, with an AQY of about 0.50% at 420 nm.[93]

In summary, considerable progress has been made for this approach

recently, which the highest AQY of 0.80% at 440 nm has been achieved until now (Table 2).[75] It is highlighted that both photocatalysts and solid-state electron mediators are vital to the Z-scheme process. To ensure an efficient charge transfer among these units, an effective interfacial contact is required. However, in most powder suspension systems the contact among the introduced metal chalcogenide photocatalyst, an OEP and a solid-state electron mediator is poor, which is mainly based on the electrostatic attractive force regulated by tuning the pH value of the reaction solution.[101] In this case, the loose contact probably limits the interparticle charge transfer during the photocatalytic reaction. Therefore, it will be highly desirable to develop an upgraded system with a more intimate contact, such as an ohmic contact with low interfacial resistance, to conquer the low charge separation efficiency for this kind of systems. The photocatalyst sheet system is one of such advanced systems, which will be introduced detailly in the following section.[14]

Solid-state electron mediator in a sheet system

Recently, the photocatalyst sheet system has been emerging as an advanced approach to achieve efficient and scalable photocatalytic Z-scheme OWS, in which HEP and OEP particles were embedded in a conductive layer acting as a solid-state electron mediator.[51,52] This approach does not require the addition of any electrolyte to the reaction solution, and the photocatalysts

fixed in an integrated device can be easily collected and replaced when necessary, both of which are advantageous to the design of practical solar OWS units.[23,53] More importantly, this system was found to split pure water much more efficiently than the powder suspension system, because the underlying rigid conductive layer could ensure efficient electron transfer from the OEP to the HEP, much higher than the case of electron transfer occurring via the aggregation of particles by attractive electrostatic forces. In addition, the photocatalyst sheet has a higher operable tolerability in pH values of the reaction solution, since the photocatalysts are fixed and integrated in one device. In this system, a particle transfer method is popularly used for the construction of the systems, and various conductive electrical conductors have been evaluated as solid-state electron mediators, such as Au, Rh, Ni, C, and ITO.[23,51,54,102] Up until now, Cr_2O_3/Ru-loaded $SrTiO_3$:La,Rh|C|$BiVO_4$:Mo sheet system has been reported to show the highest Z-scheme OWS performance, with an STH value as high as of 1.2% at 331 K and 10 kPa, which is promising to be further improved by using narrow band gap semiconductors.[23]

Metal chalcogenides is one kind of narrow band gap semiconductors. However, it suffers from severe photocorrosion during the photocatalytic reaction. How to efficiently consume photogenerated holes from the metal chalcogenides for the Z-scheme process rather than the self-oxidization reaction is a key issue for its application to OWS.[82,103] The photocatalyst sheet system offers a probable solution to this problem, because the feature of low

interfacial resistance can enable efficient interparticle charge transfer, avoiding the accumulation of holes in metal chalcogenides for the self-oxidization reaction. In 2019, our group had successfully achieved the stable Z-scheme OWS process over the photocatalyst sheet system composed of solid solutions of zinc selenide and copper gallium selenide (denoted as ZnSe:CGSe) as HEPs, $CoO_x/BiVO_4$ and Au as an OEP and an electron mediator, respectively (Figure 7A).[31] As shown in Figure 7B, both HEP and OEP particles are well-distributed and anchored in the Au layer, with a thickness of approximate 500 nm. In this system, photogenerated holes in ZnSe:CGSe can be efficiently recombined with electrons from $BiVO_4$ via the Au layer, thus avoiding self-oxidation of ZnSe:CGSe and leading to stable OWS. This is the first example of particulate metal selenides for photocatalytic OWS. More interestingly, the band structures (absorption edges ranging from 480 to 750 nm) and semiconductor characteristics of ZnSe:CGSe could be finely tuned by changing the molar ratios of Zn/(Zn + Cu) and Ga/Cu. Similar to the case of RGO electron mediator, it was identified that the p-type semiconductor character of ZnSe:CGSe and the presence of a potential window in which the ZnSe:CGSe photocathode and the $CoO_x/BiVO_4$ photoanode could generate photocurrent were essential to forming a Z-scheme process (Figure 7C).[31,33] The stability test showed that the optimal ZnSe:CGSe|Au|$BiVO_4$ sheet could split water in a stable manner over a span of 17 h under visible light irradiation, with an AQY of 0.54% at 420 nm (Figure 7D). This kind of sheet systems provides an effective approach to stabilize

photocatalytic Z-scheme OWS with metal chalcogenide photocatalysts.

Although metal chalcogenides with narrow band gaps had been successfully demonstrated to be applied in photocatalyst sheet systems for Z-scheme OWS, the poor charge separation and the sluggish catalytic kinetics are the major limitations for the low AQY at present.[31] To tackle those challenges, recently our group has constructed a p-n junction of CdS-$(ZnSe)_{0.5}(CuGa_{2.5}Se_{4.25})_{0.5}$ (denoted as CdS-ZCGSe) to enhance charge separation, together with a thin TiO_2 coating layer to prohibit the reverse reaction of OWS.[32] Photocatalytic Z-scheme OWS activity showed that the rate was improved significantly after the dual modifications with CdS and TiO_2, which was 3.2-fold greater than that for the pristine case (Figure 8A). An AQY of 1.5% at 420 nm was obtained, which was by far the highest value among the reported particulate photocatalytic Z-scheme OWS systems with metal chalcogenides as HEPs (Table 2). Long-term test of the optimized sample manifested that it could stably split water for 10 h under visible light irradiation (Figure 8B). Transient absorption spectroscopy data verified that the dual modification of TiO_2 and CdS could efficiently extract photoexcited electrons and separate them from holes in the sheet sample (Figures 8C and D). Detailed investigation further identified that the coated TiO_2 layer not only played a key role in protecting CdS from being photocorroded, but also could suppress the backward reaction of water formation from H_2 and O_2 gases during the OWS process (Figures 8E and F).[104,105] These ideas of enhanced charge separation

by p-n junction, stabilized metal chalcogenides and prohibited the reverse reaction by TiO_2 passivation layer are expected to be used as an important reference for the development of other promoted photocatalytic systems with photocorroded semiconductors.

It is worthy noting that metal chalcogenides in photocatalyst sheet systems for Z-scheme OWS only initiated in 2019, but its development is very rapid, which the presently recorded AQY of 1.5% at 420 nm is even higher than efficiencies reported in the powder suspension systems with an aqueous redox mediator or a solid-state electron mediator (Table 2). As illustrated in the aforementioned parts, how to improve the charge carriers utilization while suppress the photocorrosion of metal chalcogenides is the current key to construct efficient Z-scheme sheet systems. Our recent work of p-n junction and TiO_2 passivation layer provides a solution to address these issues.[32] However, there still exists a large room to further improve the photocatalytic systems. It is believed precise preparation of metal chalcogenides with tailored composition, structure, crystallinity, morphology and particle size will boost its advances in this approach.[12]

CONCLUSION AND PERSPECTIVES

The most important progress and guiding principles related to Z-scheme OWS using metal chalcogenide photocatalysts as the HEPs have been

summarized in three approaches: aqueous redox mediator or solid-state electron mediator in a powder suspension system, solid-state electron mediator in a sheet system. In this field, although the research history is relatively short, its progress is very rapid. Among the investigated metal chalcogenide semiconductors, various metal sulfides and metal selenides have been developed and constructed for Z-scheme OWS, with the recorded AQY of 1.5% at 420 nm. Although the present efficiency is not so high, the feature of narrow band gap of metal chalcogenides endows it with much room for the improvement. How to construct and promote its Z-scheme OWS systems is still the mainstream in the future study.

To address this challenge and boost the progress, following aspects should be carefully considered together with some series of the recommended suggestions. **(1) Development of metal chalcogenide HEPs.** In this regard, how to develop metal chalcogenide photocatalysts with enhanced H_2 evolution rates and suppressive self-oxidation process is the main target. Herein, theoretical simulations adopted with machine learning, high-throughput techniques for screening multiple compositions, advanced in situ time- and space-resolved spectroscopy characterizations will facilitate the material prediction and the corresponding precisely controlled synthesis, and deepen the understanding of charge carrier behavior.[106–110] To modulate the photogenerated holes to participate in the Z-scheme process rather than decompose itself, three following aspects over metal chalcogenide HEPs need

to be specially paid attention to: I) preparation of stable metal chalcogenides by creation of effective oxidation catalytic sites; II) construction of efficient cocatalysts for the reductant oxidation reaction; III) surface nanolayer modification to passivate metal chalcogenides. **(2) Development of OEPs with narrow band gaps.** One prominent feature of metal chalcogenide HEPs is narrow band gap. For example, the absorption edge can be tuned from 480 to 750 nm by varying the composition of ZnSe:CGSe.[31] However, at present most of the coupled OEPs are $BiVO_4$ and Bi_2MoO_6, whose absorption edges are below 520 nm, limiting the theoretical STH conversion efficiency (Table 2)[75,91]. Assuming the absorption edge of the HEP is 750 nm and the AQY is 100%, it is calculated that the theoretical STH conversion efficiency is 4.8% when it was coupled parallelly with $BiVO_4$ (Figure 9). However, the STH value can be significantly improved to 14.7%, if the OEP is replaced by the one with an absorption edge of 750 nm. Therefore, development of efficient OEPs with narrower band gaps is highly desirable. **(3) Innovation of the integrated systems.** Besides metal chalcogenide HEPs and OEPs, the construction of the integrated Z-scheme systems also needs to be innovated. For instance, if the configuration is a tandem style, the same theoretical STH value of 14.7% can be obtained with an HEP possessing an absorption edge of 750 nm, but the required absorption edge of the coupled OEP is only 583 nm (Figure 9). However, if they are assembled in a parallel form, only an STH value of 7.4% can be theoretically achieved, demonstrating the importance of configuration in

the construction of the integrated systems.[111] In addition, the solid electron mediator and surface coating layer also need to be rationally designed and incorporated, mainly in consideration of the effective interfacial charge transfer and the inhibition of side reactions listed in Table 1, both of which are key to enable efficient OWS at atmospheric pressure.[23,54,112]

Sunlight-driven OWS by particulate photocatalysts has attracted extensive attention as a scalable, low-cost approach to green hydrogen production. Recently, it has been demonstrated the feasibility to drive photocatalytic OWS process with an AQY close to 100% and to achieve practical hydrogen production via photocatalytic OWS with an illumination area of 100 m^2, which is by far the largest photocatalytic hydrogen production unit yet reported.[113,114] These works brighten the future of large-scaled photocatalytic OWS. Since the applied $SrTiO_3$:Al photocatalyst in those works only responds ultra-violet light, it is highly desired to explore new materials with narrow band gaps and excellent photocatalytic functionality, among which metal chalcogenides illustrated in this paper is one kind of such promising candidates.[115,116] It is our sincere hope that this review will motivate more scientists from different disciplines to join this exciting field, and attract multidisciplinary collaborations to cohere the research community to further speed its progress in both fundamentals and applications.

ACKNOWLEDGEMENTS

This work was financially supported by National Natural Science Foundation of China (22272082, 21925206), the Fundamental Research Funds for the Central Universities, Nankai University (63213098) and Foundation from Hebei Provincial Department of Science and Technology (226Z4307G).

AUTHOR CONTRIBUTIONS

F.Z. and K.D. supervised the preparation of this paper. F.Z., S.C. and C.L. conceived the topic of this review and wrote the manuscript. All of the authors discussed and revised the manuscript.

DECLARATION OF INTERESTS

K.D. is an advisory board member of this journal.

REFERENCES

1. Tachibana, Y., Vayssieres, L., and Durrant, J.R. (2012). Artificial photosynthesis for solar water-splitting. Nat. Photonics *6*, 511–518.

2. Pinaud, B.A., Benck, J.D., Seitz, L.C., Forman, A.J., Chen, Z., Deutsch, T.G., James, B.D., Baum, K.N., Baum, G.N., Ardo, S., et al. (2013). Technical and economic feasibility of centralized facilities for solar hydrogen production via photocatalysis and photoelectrochemistry. Energy Environ. Sci. *6*, 1983–2002.

3. Kim, D., Sakimoto, K.K., Hong, D., and Yang, P. (2015). Artificial photosynthesis for sustainable fuel and chemical production. Angew. Chem. Int. Ed. *54*, 3259–3266.

4. Segev, G., Kibsgaard, J., Hahn, C., Xu, Z.J., Cheng, W.H., Deutsch, T.G., Xiang, C., Zhang, J.Z., Hammarstrom, L., Nocera, D.G., et al. (2022). The 2022 solar fuels roadmap. J. Phys. D: Appl. Phys. *55*, 323003.

5. Xu, Y., Tountas, A.A, Song, R., Ye, J., Wei, J., Ji, S., Zhao, L., Zhou, W., Chen, J., Zhao, G., et al. (2023). Equilibrium photo-thermodynamics enables a sustainable methanol synthesis. Joule *7*, 738–752.

6. Hisatomi, T., and Domen, K. (2023). Overall water splitting: What's next? Next Energy *1*, 100006.

7. Wang, W., Wang, S., Ma, X., and Gong, J. (2011). Recent advances in catalytic hydrogenation of carbon dioxide. Chem. Soc. Rev. *40*, 3703–3727.

8. Wang, J., Li, G., Li, Z., Tang, C., Feng, Z., An, H., Liu, H., Liu, T., and Li, C. (2017). A highly selective and stable ZnO-ZrO_2 solid solution catalyst for CO_2 hydrogenation to methanol. Sci. Adv. *3*, e1701290.

9. Shih, C., Zhang, T., Li, J., and Bai, C. (2018). Powering the future with liquid sunshine. Joule *2*, 1925–1949.

10. Fabian, D.M., Hu, S., Singh, N., Houle, F.A., Hisatomi, T., Domen, K., Osterloh, F.E., and Ardo, S. (2015). Particle suspension reactors and materials for solar-driven water splitting. Energy Environ. Sci. *8*, 2825–2850.

11. Kim, J., Hansora, D., Sharma, P., Jang, J., and Lee, J. (2018). Toward practical solar hydrogen production - an artificial photosynthetic leaf-to-farm challenge. Chem. Soc. Rev. *48*, 1908–1971.

12. Tao, X., Zhao, Y., Wang, S., Li, C., and Li, R. (2022). Recent advances and perspectives for solar-driven water splitting using particulate photocatalysts. Chem. Soc. Rev. *51*, 3561–3608.

13. Zhou, P., Navid, I.A., Ma, Y., Xiao, Y., Wang, P., Ye, Z., Zhou, B., Sun, K., and Mi, Z. (2023). Solar-to-hydrogen efficiency of more than 9% in photocatalytic water splitting. Nature *613*, 66–70.

14. Wang, Q., and Domen, K. (2020). Particulate photocatalysts for light-driven water splitting: mechanisms, challenges, and design strategies. Chem. Rev. *120*, 919–985.

15. Wang, Z., Hisatomi, T., Li, R., Sayama, K., Liu, G., Domen, K., Li, C., and Wang, L. (2021). Efficiency accreditation and testing protocols for particulate photocatalysts toward solar fuel production. Joule *5*, 344–359.

16. Li, H., Tu, W., Zhou, Y., and Zou, Z. (2016). Z-scheme photocatalytic systems for promoting photocatalytic performance: recent progress and future challenges. Adv. Sci. *3*, 1500389.

17. Chen, S., Takata, T., and Domen, K. (2017). Particulate photocatalysts for overall water splitting. Nat. Rev. Mater. *2*, 17050.

18. Kudo, A. (2011). Z-scheme photocatalyst systems for water splitting under visible light irradiation. MRS Bull. *36*, 32–38.

19. Maeda, K. (2013). Z-scheme water splitting using two different semiconductor photocatalysts. ACS Catal. *3*, 1486–1503.

20. Fujito, H., Kunioku, H., Kato, D., Suzuki, H., Higashi, M., Kageyama, H., and Abe, R. (2016). Layered perovskite oxychloride Bi_4NbO_8Cl: a stable visible light responsive

photocatalyst for water splitting. J. Am. Chem. Soc. *138*, 2082–2085.

21. Wang, Y., Suzuki, H., Xie, J., Tomita, O., Martin, D.J., Higashi, M., Kong, D., Abe, R., and Tang, J. (2018). Mimicking natural photosynthesis: solar to renewable H_2 fuel synthesis by Z-scheme water splitting systems. Chem. Rev. *118*, 5201–5241.

22. Pan, Z., Zhang, G., and Wang, X. (2019). Polymeric carbon nitride/reduced graphene oxide/Fe_2O_3: all-solid-state Z-scheme system for photocatalytic overall water splitting. Angew. Chem. Int. Ed. *58*, 7102–7106.

23. Wang, Q., Hisatomi, T., Suzuki, Y., Pan, Z., Seo, J., Katayama, M., Minegishi, T., Nishiyama, H., Takata, T., Seki, K., et al. (2017). Particulate photocatalyst sheets based on carbon conductor layer for efficient Z-scheme pure-water splitting at ambient pressure. J. Am. Chem. Soc. *139*, 1675–1683.

24. Bouroushian, M. (2010). Chalcogens and metal chalcogenides. In Electrochemistry of Metal Chalcogenides, M. Bouroushian, ed. (Springer Berlin Heidelberg), pp. 1–56.

25. Rahman, A., and Khan, M.M. (2021). Chalcogenides as photocatalysts. New J. Chem. *45*, 19622–19635.

26. Guillemoles, J.F., Kronik, L., Cahen, D., Rau, U., Jasenek, A., and Schock, H.W. (2000). Stability issues of Cu(In,Ga)Se_2-based solar cells. J. Phys. Chem. B *104*, 4849–4862.

27. Zhang, L., Minegishi, T., Kubota, J., and Domen, K. (2014). Hydrogen evolution from water using $Ag_xCu_{1-x}GaSe_2$ photocathodes under visible light. Phys. Chem. Chem. Phys. *16*, 6167–6174.

28. Zhu, Q., Xu, Q., Du, M., Zeng, X., Zhong, G., Qiu, B., and Zhang, J. (2022). Recent progress of metal sulfide photocatalysts for solar energy conversion. Adv. Mater. *34*, 2202929.

29. Green, M.A., Dunlop, E.D., Siefer, G., Yoshita, M., Kopidakis, N., Bothe, K., and Hao, X. (2023). Solar cell efficiency tables (Version 61). Prog. Photovolt. Res. Appl. *31*, 3–16.

30. Iwashina, K., Iwase, A., Ng, Y.H., Amal, R., and Kudo, A. (2015). Z-schematic water splitting into H_2 and O_2 using metal sulfide as a hydrogen-evolving photocatalyst and reduced graphene oxide as a solid-state electron mediator. J. Am. Chem. Soc. *137*, 604–607.

31. Chen, S., Ma, G., Wang, Q., Sun, S., Hisatomi, T., Higashi, T., Wang, Z., Nakabayashi, M., Shibata, N., Pan, Z., et al. (2019). Metal selenide photocatalysts for visible-light-driven Z-scheme pure water splitting. J. Mater. Chem. A *7*, 7415–7422.

32. Chen, S., Vequizo, J.J.M., Pan, Z., Hisatomi, T., Nakabayashi, M., Lin, L., Wang, Z., Kato, K., Yamakata, A., Shibata, N., et al. (2021). Surface modifications of $(ZnSe)_{0.5}(CuGa_{2.5}Se_{4.25})_{0.5}$ to promote photocatalytic Z-scheme overall water splitting. J. Am. Chem. Soc. *143*, 10633–10641.

33. Iwase, A., Yoshino, S., Takayama, T., Ng, Y.H., Amal, R., and Kudo, A. (2016). Water splitting and CO_2 reduction under visible light irradiation using Z-scheme systems consisting of metal sulfides, CoO_x-loaded $BiVO_4$, and a reduced graphene oxide electron mediator. J. Am. Chem. Soc. *138*, 10260–10264.

34. Ren, Y., Foo, J.J., Zeng, D., and Ong, W.J. (2022). $ZnIn_2S_4$-based nanostructures in artificial photosynthesis: insights into photocatalytic reduction toward sustainable energy production. Small Struct. *3*, 2200017.

35. Chong, W.K., Ng, B.J., Tan, L.L., and Chai, S.P. (2022). Recent advances in nanoscale engineering of ternary metal sulfide-based heterostructures for photocatalytic water splitting applications. Energy Fuels *36*, 4250–4267.

36. Fujishima, A., and Honda, K. (1972). Electrochemical photolysis of water at a semiconductor electrode. Nature *238*, 37–38.

37. Kudo, A., and Miseki, Y. (2009). Heterogeneous photocatalyst materials for water splitting. Chem. Soc. Rev. *38*, 253–278.

38. Abe, R., Sayama, K., Domen, K., and Arakawa, H. (2001). A new type of water splitting system composed of two different TiO_2 photocatalysts (anatase, rutile) and a IO_3^-/I^- shuttle redox mediator. Chem. Phys. Lett. *344*, 339–344.

39. Bard, A.J. (1979). Photoelectrochemistry and heterogeneous photo-catalysis at semiconductors. J. Photochem. *10*, 59–75.

40. Kato, H., Sasaki, Y., Shirakura, N., and Kudo, A. (2013). Synthesis of highly active rhodium-doped $SrTiO_3$ powders in Z-scheme systems for visible-light-driven photocatalytic overall water splitting. J. Mater. Chem. A *1*, 12327–12333.

41. Sasaki, Y., Kato, H., and Kudo, A. (2013). $[Co(bpy)_3]^{3+/2+}$ and $[Co(phen)_3]^{3+/2+}$ electron mediators for overall water splitting under sunlight irradiation using Z-scheme photocatalyst system. J. Am. Chem. Soc. *135*, 5441–5449.

42. Chen, S., Qi, Y., Hisatomi, T., Ding, Q., Asai, T., Li, Z., Ma, S.S.K., Zhang, F., Domen, K., and Li, C. (2015). Efficient visible-light-driven Z-scheme overall water splitting using a $MgTa_2O_{6-x}N_y$/TaON heterostructure photocatalyst for H_2 evolution. Angew. Chem. Int. Ed. *54*, 8498–8501.

43. Kato, T., Hakari, Y., Ikeda, S., Jia, Q., Iwase, A., and Kudo, A. (2015). Utilization of metal sulfide material of $(CuGa)_{1-x}Zn_{2x}S_2$ solid solution with visible light response in photocatalytic and photoelectrochemical solar water splitting systems. J. Phys. Chem. Lett. *6*, 1042–1047.

44. Tsuji, K., Tomita, O., Higashi, M., and Abe, R. (2016). Manganese-substituted polyoxometalate as an effective shuttle redox mediator in Z-scheme water splitting under visible light. ChemSusChem *9*, 2201–2208.

45. Ma, G., Chen, S., Kuang, Y., Akiyama, S., Hisatomi, T., Nakabayashi, M., Shibata, N., Katayama, M., Minegishi, T., and Domen, K. (2016). Visible light-driven Z-scheme

water splitting using oxysulfide H_2 evolution photocatalysts. J. Phys. Chem. Lett. *7*, 3892–3896.

46. Miseki, Y., Fujiyoshi, S., Gunji, T., and Sayama, K. (2017). Photocatalytic Z-scheme water splitting for independent H_2/O_2 production via a stepwise operation employing a vanadate redox mediator under visible light. J. Phys. Chem. C *121*, 9691–9697.

47. Iwase, Y., Tomita, O., Naito, H., Higashi, M., and Abe, R. (2018). Molybdenum-substituted polyoxometalate as stable shuttle redox mediator for visible light driven Z-scheme water splitting system. J. Photochem. Photobiol. A Chem. *356*, 347–354.

48. Qi, Y., Zhang, J., Kong, Y., Zhao, Y., Chen, S., Li, D., Liu, W., Chen, Y., Xie, T., Cui, J., et al. (2022). Unraveling of cocatalysts photodeposited selectively on facets of $BiVO_4$ to boost solar water splitting. Nat. Commun. *13*, 484.

49. Tada, H., Mitsui, T., Kiyonaga, T., Akita, T., and Tanaka, K. (2006). All-solid-state Z-scheme in CdS–Au–TiO_2 three-component nanojunction system. Nat. Mater. *5*, 782–786.

50. Sasaki, Y., Nemoto, H., Saito, K., and Kudo, A. (2009). Solar water splitting using powdered photocatalysts driven by Z-schematic interparticle electron transfer without an electron mediator. J. Phys. Chem. C *113*, 17536–17542.

51. Wang, Q., Li, Y., Hisatomi, T., Nakabayashi, M., Shibata, N., Kubota, J., and Domen, K. (2015). Z-scheme water splitting using particulate semiconductors immobilized onto metal layers for efficient electron relay. J. Catal. *328*, 308–315.

52. Wang, Q., Hisatomi, T., Jia, Q., Tokudome, H., Zhong, M., Wang, C., Pan, Z., Takata, T., Nakabayashi, M., Shibata, N., et al. (2016). Scalable water splitting on particulate photocatalyst sheets with a solar-to-hydrogen energy conversion efficiency exceeding 1%. Nat. Mater. *15*, 611–615.

53. Wang, Q., Hisatomi, T., Katayama, M., Takata, T., Minegishi, T., Kudo, A., Yamada, T., and Domen, K. (2017). Particulate photocatalyst sheets for Z-scheme water splitting: advantages over powder suspension and photoelectrochemical systems and future challenges. Faraday Discuss. *197*, 491–504.

54. Wang, Q., Okunaka, S., Tokudome, H., Hisatomi, T., Nakabayashi, M., Shibata, N., Yamada, T., and Domen, K. (2018). Printable photocatalyst sheets incorporating a transparent conductive mediator for Z-scheme water splitting. Joule, *2*, 2667–2680.

55. Srinivasan, N., Sakai, E., and Miyauchi, M. (2016). Balanced excitation between two semiconductors in bulk heterojunction Z-scheme system for overall water splitting. ACS Catal. *6*, 2197–2200.

56. Kobayashi, R., Takashima, T., Tanigawa, S., Takeuchi, S., Ohtani, B., and Irie, H. (2016). A heterojunction photocatalyst composed of zinc rhodium oxide, single crystal-derived bismuth vanadium oxide, and silver for overall pure-water splitting under visible light up to 740 nm. Phys. Chem. Chem. Phys. *18*, 27754–27760.

57. Wang, Q., Hisatomi, T., Ma, S., Li, Y., and Domen, K. (2014). Core/shell structured La and Rh-codoped $SrTiO_3$ as a hydrogen evolution photocatalyst in Z-scheme overall water splitting under visible light irradiation. Chem. Mater. *26*, 4144–4150.

58. Iwase, A., Ng, Y.H., Ishiguro, Y., Kudo, A., and Amal, R. (2011). Reduced graphene oxide as a solid-state electron mediator in Z-scheme photocatalytic water splitting under visible light. J. Am. Chem. Soc. *133*, 11054–11057.

59. Abe, R. (2011). Development of a new system for photocatalytic water splitting into H_2 and O_2 under visible light irradiation. Bull. Chem. Soc. Jpn. *84*, 1000–1030.

60. Stroyuk, O., Raevskaya, A., and Gaponik, N. (2018). Solar light harvesting with multinary metal chalcogenide nanocrystals. Chem. Soc. Rev. *47*, 5354–5422.

61. Nie, L., and Zhang, Q. (2017). Recent progress in crystalline metal chalcogenides as efficient photocatalysts for organic pollutant degradation. Inorg. Chem. Front. *4*, 1953–1962.

62. Yuan, Q., Liu, D., Zhang, N., Ye, W., Ju, H., Shi, L., Long, R., Zhu, J., and Xiong, Y. (2017). Noble-metal-free janus-like structures by cation exchange for Z-scheme photocatalytic water splitting under broadband light irradiation. Angew. Chem. Int. Ed. *56*, 4206–4210.

63. Wei, Z., Liu, J., and Shangguan, W. (2020). A review on photocatalysis in antibiotic wastewater: pollutant degradation and hydrogen production. Chin. J. Catal. *41*, 1440–1450.

64. Liu, F., Xue, F., Si, Y., Chen, G., Guan, X., Lu, K., and Liu, M. (2021). Functionalized $Cd_{0.5}Zn_{0.5}S$ chalcogenide nanotwins enabling Z-scheme photocatalytic water splitting. ACS Appl. Nano Mater. *4*, 759–768.

65. Wu, X., Xie, S., Zhang, H., Zhang, Q., Sels, B., and Wang, Y. (2021). Metal sulfide photocatalysts for lignocellulose valorization. Adv. Mater. *33*, 2007129.

66. Jia, L., Tan, X., Yu, T., and Ye, J. (2022). Mixed metal sulfides for the application of photocatalytic energy conversion. Energy Fuels *36*, 11308–11322.

67. Bai, S., Qiu, H., Song, M., He, G., Wang, F., Liu, Y., and Guo, L. (2022). Porous fixed-bed photoreactor for boosting C–C coupling in photocatalytic CO_2 reduction. eScience *42*, 428–437.

68. Zhang, K., and Guo, L. (2013). Metal sulphide semiconductors for photocatalytic hydrogen production. Catal. Sci. Technol. *3*, 1672–1690.

69. Tsuji, I., Kato, H., Kobayashi, H., and Kudo, A. (2004). Photocatalytic H_2 evolution reaction from aqueous solutions over band structure-controlled $(AgIn)_xZn_{2(1-x)}S_2$ solid solution photocatalysts with visible-light response and their surface nanostructures. J. Am. Chem. Soc. *126*, 13406–13413.

70. Dong, B., Liu, T., Li, C., and Zhang, F. (2018). Species, engineering and

characterizations of defects in TiO_2-based photocatalyst. Chin. Chem. Lett. *29*, 671–680.

71. Tsuji, I., Kato, H., and Kudo, A. (2005). Visible-light-induced H_2 evolution from an aqueous solution containing sulfide and sulfite over a ZnS–$CuInS_2$–$AgInS_2$ solid-solution photocatalyst. Angew. Chem. Int. Ed. *44*, 3665–3668.

72. Yan, H., Yang, J., Ma, G., Wu, G., Zong, X., Lei, Z., Shi, J., and Li, C. (2009). Visible-light-driven hydrogen production with extremely high quantum efficiency on Pt–PdS/CdS photocatalyst. J. Catal. *266*, 165–168.

73. Sarilmaz, A., Can, M., and Ozel, F. (2017). Ternary copper tungsten selenide nanosheets synthesized by a facile hot-injection method. J. Alloys Compds. *699*, 479–483.

74. Khalil, A.A.I., Abd El-Gawad, A.S.H.M., and Gadallah, A.S. (2020). Impact of silver dopants on structural, morphological, optical, and electrical properties of copper-zinc sulfide thin films prepared via sol-gel spin coating method. Opt. Mater. *109*, 110250.

75. Yoshino, S., Iwase, A., Ng, Y.H., Amal, R., and Kudo, A. (2020). Z-schematic solar water splitting using fine particles of H_2-evolving $(CuGa)_{0.5}ZnS_2$ photocatalyst prepared by a flux method with chloride salts. ACS Appl. Energy Mater. *3*, 5684–5692.

76. Chen, S., Vequizo, J.J.M., Hisatomi, T., Nakabayashi, M., Lin, L., Wang, Z., Yamakata, A., Shibata, N., Takata, T., Yamada, T., et al. (2020). Efficient photocatalytic hydrogen evolution on single-crystalline metal selenide particles with suitable cocatalysts. Chem. Sci. *11*, 6436–6441.

77. Pan, R., Hu, M., Liu, J., Li, D., Wan, X., Wang, H., Li, Y., Zhang, X., Wang, X., Jiang, J., et al. (2021). Two-dimensional all-in-one sulfide monolayers driving photocatalytic overall water splitting. Nano Lett. *21*, 6228–6236.

78. Yang, J., Yan, H., Wang, X., Wen, F., Wang, Z., Fan, D., Shi, J., and Li, C. (2012). Roles of cocatalysts in Pt-PdS/CdS with exceptionally high quantum efficiency for photocatalytic hydrogen production. J. Catal. *290*, 151–157.

79. Wolff, C.M., Frischmann, P.D., Schulze, M., Bohn, B.J., Wein, R., Livadas, P., Carlson, M.T., Jäckel, F., Feldmann, J., Würthner, F., et al. (2018). All-in-one visible-light-driven water splitting by combining nanoparticulate and molecular co-catalysts on CdS nanorods. Nat. Energy *3*, 862–869.

80. Ning, X., Li, J., Yang, B., Zhen, W., Li, Z., Tian, B., and Lu, G. (2017). Inhibition of photocorrosion of CdS via assembling with thin film TiO_2 and removing formed oxygen by artificial gill for visible light overall water splitting. Appl. Catal. B Environ. *212*, 129–139.

81. Ning, X., and Lu, G. (2020). Photocorrosion inhibition of CdS-based catalysts for photocatalytic overall water splitting. Nanoscale *12*, 1213–1223.

82. Chen, S., Qi, Y., Li, C., Domen, K., and Zhang, F. (2018). Surface strategies for

particulate photocatalysts toward artificial photosynthesis. Joule *2*, 2260–2288.

83. Wang, W., Chen, J., Li, C., and Tian, W. (2014). Achieving solar overall water splitting with hybrid photosystems of photosystem II and artificial photocatalysts. Nat. Commun. *5*, 4647.

84. Wang, X., Zhuo, Z., Shen, C., Cai, M., Li, D., Liu, K., Cao, S., Wei, Y., Xue, Z., and Sun, S. (2023). Visible-light driven Z-scheme water splitting over NiS/CdS/PtO_x/WO_3 through modulating redox mediator environments. ChemPhotoChem *7*, e202200211.

85. Chen, S., Hisatomi, T., Ma, G., Wang, Z., Pan, Z., Takata, T., and Domen, K. (2019). Metal selenides for photocatalytic Z-scheme pure water splitting mediated by reduced graphene oxide. Chin. J. Catal. *40*, 1668–1672.

86. Domen, K., Naito, S., Soma, M., Onishi, T., and Tamaru, K. (1980). Photocatalytic decomposition of water vapour on an NiO-$SrTiO_3$ catalyst. J. Chem. Soc. Chem. Commun. 543–544.

87. Sayama, K., Mukasa, K., Abe, R., Abe, Y., and Arakawa, H. (2001). Stoichiometric water splitting into H_2 and O_2 using a mixture of two different photocatalysts and an IO_3^-/I^- shuttle redox mediator under visible light irradiation. Chem. Commun. 2416–2417.

88. Shirakawa, T., Higashi, M., Tomita, O., and Abe, R. (2017). Surface-modified metal sulfides as stable H_2-evolving photocatalysts in Z-scheme water splitting with a $[Fe(CN)_6]^{3-/4-}$ redox mediator under visible light irradiation. Sustain. Energy Fuels *1*, 1065–1073.

89. Kageshima, Y., Gomyo, Y., Matsuoka, H., Inuzuka, H., Suzuki, H., Abe, R., Teshima, K., Domen, K., and Nishikiori, H. (2021). Z-scheme overall water splitting using $Zn_xCd_{1-x}Se$ particles coated with metal cyanoferrates as hydrogen evolution photocatalysts. ACS Catal. *11*, 8004–8014.

90. Yuan, Y., Chen, D., Yang, S., Yang, L., Wang, J., Cao, D., Tu, W., Yu, Z., and Zou, Z. (2017). Constructing noble-metal-free Z-scheme photocatalytic overall water splitting systems using MoS_2 nanosheet modified CdS as a H_2 evolution photocatalyst. J. Mater. Chem. A *5*, 21205–21213.

91. Wan, S., Ou, M., Zhong, Q., Zhang, S., and Song, F. (2017). Construction of Z-scheme photocatalytic systems using $ZnIn_2S_4$, CoO_x-loaded Bi_2MoO_6 and reduced graphene oxide electron mediator and its efficient nonsacrificial water splitting under visible light. Chem. Eng. J. *325*, 690–699.

92. Wu, X., Zhao, J., Wang, L., Han, M., Zhang, M., Wang, H., Huang, H., Liu, Y., and Kang, Z. (2017). Carbon dots as solid-state electron mediator for $BiVO_4$/CDs/CdS Z-scheme photocatalyst working under visible light. Appl. Catal. B: Environ. *206*, 501–509.

93. Ding, Y., Wei, D., He, R., Yuan, R., Xie, T., and Li, Z. (2019). Rational design of Z-

scheme PtS-$ZnIn_2S_4$/WO_3-MnO_2 for overall photocatalytic water splitting under visible light. Appl. Catal. B: Environ. *258*, 117948.

94. Qi, Y., Zhao, Y., Gao, Y., Li, D., Li, Z., Zhang, F., and Li, C. (2018). Redox-based visible-light driven Z-scheme overall water splitting with apparent quantum efficiency exceeding 10%. Joule *2*, 2393–2402.

95. Li, Z., Wang, W., Ding, C., Wang, Z., Liao, S., and Li, C. (2017). Biomimetic electron transport via multiredox shuttles from photosystem II to a photoelectrochemical cell for solar water splitting. Energy Environ. Sci. *10*, 765–771.

96. Wang, W., Wang, H., Zhu, Q., Qin, W., Han, G., Shen, J., Zong, X., and Li, C. (2016). Spatially separated photosystem II and a silicon photoelectrochemical cell for overall water splitting: a natural–artificial photosynthetic hybrid. Angew. Chem. Int. Ed. *55*, 9229–9233.

97. Matsuoka, H., Higashi, M., Nakada, A., Tomita, O., and Abe, R. (2018). Enhanced H_2 evolution on $ZnIn_2S_4$ photocatalyst under visible light by surface modification with metal cyanoferrates. Chem. Lett. *47*, 941–944.

98. Zhang, Z., and Yates, J.T., Jr. (2012). Band bending in semiconductors: chemical and physical consequences at surfaces and interfaces. Chem. Rev. *112*, 5520–5551.

99. Li, S., Zhao, Q., Wang, D., and Xie, T. (2016). Work function engineering derived all-solid-state Z-scheme semiconductor-metal-semiconductor system towards high-efficiency photocatalytic H_2 evolution. RSC Adv. *6*, 66783–66787.

100. Hisatomi, T., Kubota, J., and Domen, K. (2014). Recent advances in semiconductors for photocatalytic and photoelectrochemical water splitting. Chem. Soc. Rev. *43*, 7520–7535.

101. Ma, S.S.K., Maeda, K., Hisatomi, T., Tabata, M., Kudo, A., and Domen, K. (2013). A redox-mediator-free solar-driven Z-scheme water-splitting system consisting of modified Ta_3N_5 as an oxygen-evolution photocatalyst. Chem. Eur. J. *19*, 7480–7486.

102. Minegishi, T., Nishimura, N., Kubota, J., and Domen, K. (2013). Photoelectrochemical properties of $LaTiO_2N$ electrodes prepared by particle transfer for sunlight-driven water splitting. Chem. Sci. *4*, 1120–1124.

103. Zhou, P., Yu, J., and Jaroniec, M. (2014). All-solid-state Z-scheme photocatalytic systems. Adv. Mater. *26*, 4920–4935.

104. Pan, Z., Hisatomi, T., Wang, Q., Chen, S., Nakabayashi, M., Shibata, N., Pan, C., Takata, T., Katayama, M., Minegishi, T., et al. (2016). Photocatalyst sheets composed of particulate $LaMg_{1/3}Ta_{2/3}O_2N$ and Mo-doped $BiVO_4$ for Z-scheme water splitting under visible light. ACS Catal. *6*, 7188–7196.

105. Takata, T., Pan, C., Nakabayashi, M., Shibata, N., and Domen, K. (2015). Fabrication of a core-shell-type photocatalyst via photodeposition of group IV and V transition metal oxyhydroxides: an effective surface modification method for overall water

splitting. J. Am. Chem. Soc. *137*, 9627–9634.

106. Chen, R., Fan, F., Dittrich, T., and Li, C. (2018). Imaging photogenerated charge carriers on surfaces and interfaces of photocatalysts with surface photovoltage microscopy. Chem. Soc. Rev. *47*, 8238–8262.

107. Masood, H., Toe, C.Y., Teoh, W.Y., Sethu, V., and Amal, R. (2019). Machine learning for accelerated discovery of solar photocatalysts. ACS Catal. *9*, 11774–11787.

108. Li, X., Maffettone, P.M., Che, Y., Liu, T., Chen, L., and Cooper, A.I. (2021). Combining machine learning and high-throughput experimentation to discover photocatalytically active organic molecules. Chem. Sci. *12*, 10742–10754.

109. Mai, H., Le, T.C., Chen, D., Winkler, D.A., and Caruso, R.A. (2022). Machine learning for electrocatalyst and photocatalyst design and discovery. Chem. Rev. *122*, 13478–13515.

110. Chen, R., Ren, Z., Liang, Y., Zhang, G., Dittrich, T., Liu, R., Liu, Y., Zhao, Y., Pang, S., An, H., et al. (2022). Spatiotemporal imaging of charge transfer in photocatalyst particles. Nature *610*, 296–301.

111. Dong, C., Zhao, Y., Luo, Y., Wang, H., Zhang, H., Zong, X., Feng, Z., and Li, C. (2022) Designing a Z-scheme system based on photocatalyst panels towards separated hydrogen and oxygen production from overall water splitting. Catal. Sci. Technol. *12*, 572–578.

112. Nandy, S., Hisatomi, T., Nakabayashi, M., Li, H., Wang, X., Shibata, N., Takata, T., and Domen, K. (2023) Oxide layer coating enabling oxysulfide-based photocatalyst sheet to drive Z-scheme water splitting at atmospheric pressure. Joule *7*, 1641–1651.

113. Takata, T., Jiang, J., Sakata, Y., Nakabayashi, M., Shibata, N., Nandal, V., Seki, K., Hisatomi, T., and Domen, K. (2020). Photocatalytic water splitting with a quantum efficiency of almost unity. Nature *581*, 411–414.

114. Nishiyama, H., Yamada, T., Nakabayashi, M., Maehara, Y., Yamaguchi, M., Kuromiya, Y., Nagatsuma, Y., Tokudome, H., Akiyama, S., Watanabe, T., et al. (2021). Photocatalytic solar hydrogen production from water on a 100 m^2-scale. Nature *598*, 304–307.

115. Xiao, J., Hisatomi, T., and Domen, K. (2023). Narrow-band-gap particulate photocatalysts for one-step-excitation overall water splitting. Acc. Chem. Res. *56*, 878–888.

116. Nishioka, S., Osterloh, F.E., Wang, X., Mallouk, T.E., and Maeda, K. (2023). Photocatalytic water splitting. Nat. Rev. Methods Primers *3*, 42.

Figure 1. Schematic energy diagrams for different types of photocatalytic Z-scheme overall water-splitting systems with metal chalcogenide HEPs

(A) Z-scheme system with an aqueous redox mediator.

(B) Z-scheme system with a solid-state electron mediator.

VB, valence band; CB, conduction band; E_g, semiconductor bandgap; HEP, H_2 evolution photocatalyst; NHE, normal hydrogen electrode; OEP, O_2 evolution photocatalyst; Ox, oxidant; Red, reductant.

Figure 2. Band structure of metal chalcogenides

(A) Elements in the periodic table used to construct most of the metal chalcogenide photocatalysts for Z-scheme overall water-splitting and their roles.

(B) Schematic figure of band structure of the general metal chalcogenides. Herein, only the major contribution from atomic orbitals to the band edges is given.

(C) Band positions of some typical metal chalcogenides.

CBM, conduction band minimum; VBM, valence band maximum.

Figure 3. Timeline of the key developments in photocatalytic Z-scheme OWS using metal chalcogenide photocatalysts

OWS, overall water splitting; PEC, photoelectrochemical; RGO, reduced graphene oxide.

Figure 4. Z-scheme OWS over a PSII-photocatalyst hybrid system

(A) Schematic of the reaction mechanism.

(B) Optical microscope image of the hybrid system of PSII-Ru_2S_3/CdS. Scale bar, 10 μm.

(C) Time course of the Z-scheme OWS reaction over PSII-Ru_2S_3/CdS.

PSII, photosystem II.

(A)–(C) are reprinted with permission from Wang et al.[83] Copyright 2014, Nature Publishing Group.

Figure 5. Schematic mechanism of H_2 evolution over a CdS photocatalyst coupled with a water oxidation photoanode

(A) Schematic illustration of the proposed Z-scheme OWS system.

(B) The reaction mechanism of H_2 evolution over Pt/CdS in the presence of $K_2[CdFe(CN)_6]$.

(A)–(B) are reprinted with permission from Shirakawa et al.[88] Copyright 2017, The Royal Society of Chemistry.

Figure 6. Z-scheme OWS with a metal sulfide photocatalyst or a photocathode

(A) The working diagram of the Z-scheme OWS system using Pt loaded metal sulfides as HEPs, $CoO_x/BiVO_4$ and RGO as an OEP and an electron mediator, respectively.

(B) Time course of H_2 and O_2 evolution over the Z-scheme system using Pt/$CuGaS_2$, and RGO-$BiVO_4$ photocatalysts with or without CoO_x under visible light.

(C) Illustration of a PEC system consisting of a metal sulfide photocathode and $CoO_x/BiVO_4$ photoanode connected by RGO for OWS without external bias.

(D) Current-potential curves of different samples in sodium phosphate buffer solution under visible light irradiation.

OWS, overall water splitting; HEP, H_2 evolution photocatalyst; OEP, O_2 evolution photocatalyst; PEC, photoelectrochemical; RGO, reduced graphene oxide.

(A)–(D) are reprinted with permission from Iwase et al.[33] Copyright 2016, American Chemical Society.

Figure 7. Photocatalytic Z-scheme OWS over a ZnSe:CGSe|Au|$BiVO_4$ sheet system

(A) Schematic diagram of the photocatalyst sheet system using Pt/Cr_2O_3/ZnSe:CGSe as an HEP, $CoO_x/BiVO_4$ and Au as an OEP and an electron mediator, respectively.

(B) SEM and SEM-EDS mapping images of the sheet system.

(C) Gas evolution rate of the ZnSe:CGSe|Au|$BiVO_4$ sheet systems with different molar ratios of Zn/(Zn + Cu).

(D) The photocatalytic stability test results of ZCGSe|Au|$BiVO_4$ sheet system under visible light irradiation.

Herein, ZCGSe denotes $(ZnSe)_{0.5}(CuGa_{2.5}Se_{4.25})_{0.5}$; OWS, overall water splitting; HEP, H_2 evolution photocatalyst; OEP, O_2 evolution photocatalyst; RGO, reduced graphene oxide.

(A)–(D) are reprinted with permission from Chen et al.[31] Copyright 2019, The Royal Society of Chemistry.

Figure 8. Photocatalytic Z-scheme OWS over a ZCGSe|Au|$BiVO_4$:Mo sheet system modified with TiO_2 and CdS

(A) The comparison of initial gas evolution rates over Pt-loaded ZCGSe|Au|$BiVO_4$:Mo samples with different modifications.

(B) Time course of gas evolution during OWS over the optimized ZCGSe|Au|$BiVO_4$:Mo sample under visible light irradiation.

(C) Decay kinetics of electrons probed at 5000 cm^{-1} (2000 nm), and (D) decay kinetics of holes monitored at 19800 cm^{-1} (505 nm) on surface-modified ZCGSe|Au|$BiVO_4$:Mo sheet samples. ((I) ZCGSe|Au|$BiVO_4$:Mo; (II) Pt-loaded ZCGSe|Au|$BiVO_4$:Mo; (III) Pt-loaded TiO_2-ZCGSe|Au|$BiVO_4$:Mo; (IV) Pt-loaded CdS-ZCGSe|Au|$BiVO_4$:Mo; (V) Pt-loaded TiO_2/CdS-ZCGSe|Au|$BiVO_4$:Mo).

(E) Effect of TiO_2 modification on the water formation reaction over the sheet system under darkness (with TiO_2 modification: spheres; without TiO_2 modification: open hexagons).

(F) Proposed working mechanism for ZCGSe|Au|$BiVO_4$:Mo sample modified with TiO_2 and CdS.

Herein, ZCGSe denotes $(ZnSe)_{0.5}(CuGa_{2.5}Se_{4.25})_{0.5}$; OWS, overall water splitting; OEP, O_2 evolution photocatalyst.

(A)–(F) are reprinted with permission from Chen et al.[32] Copyright 2021, American Chemical Society.

Figure 1

Click here to access/download;Figure;Figure 1.TIF

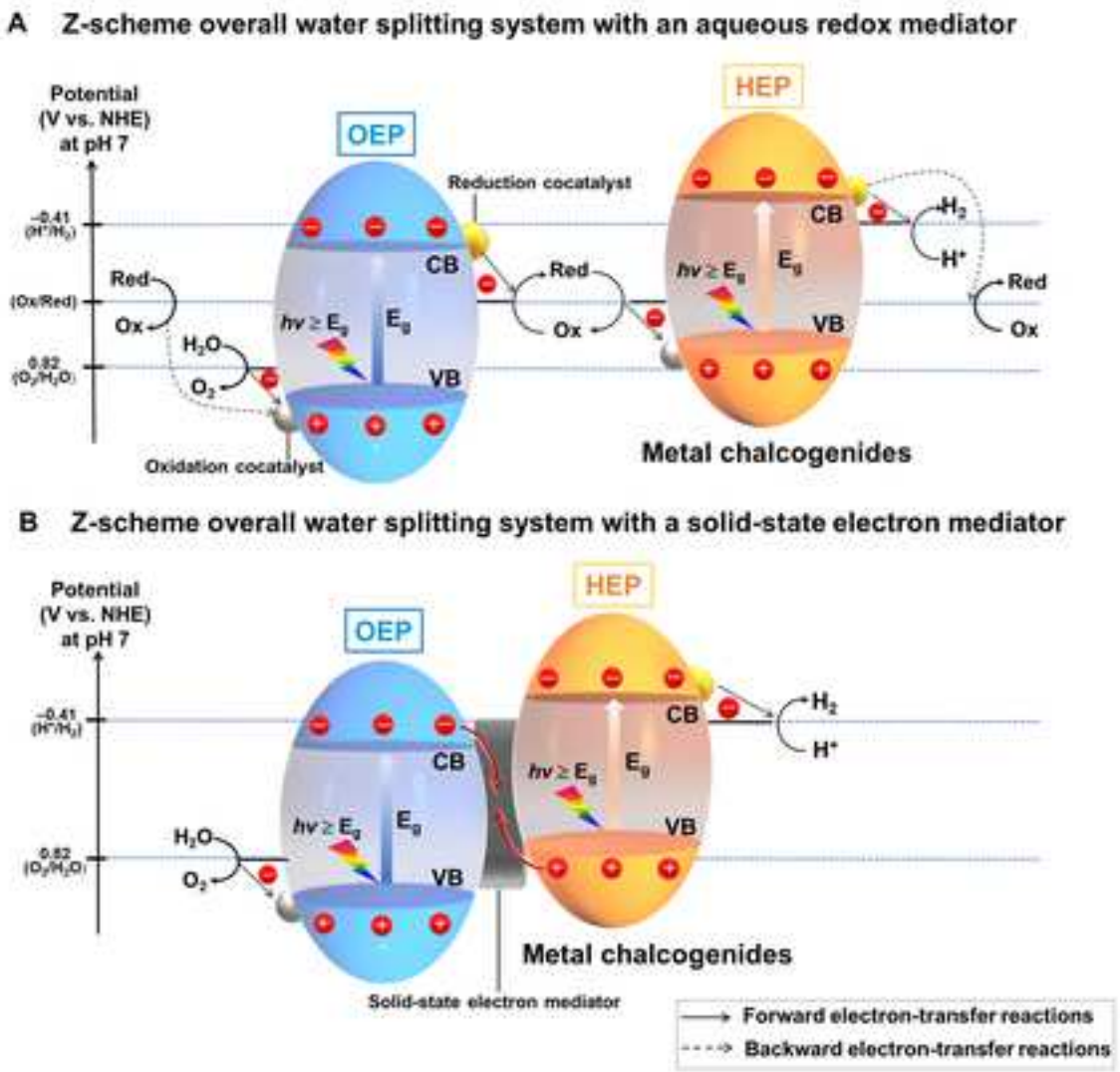

Figure 2

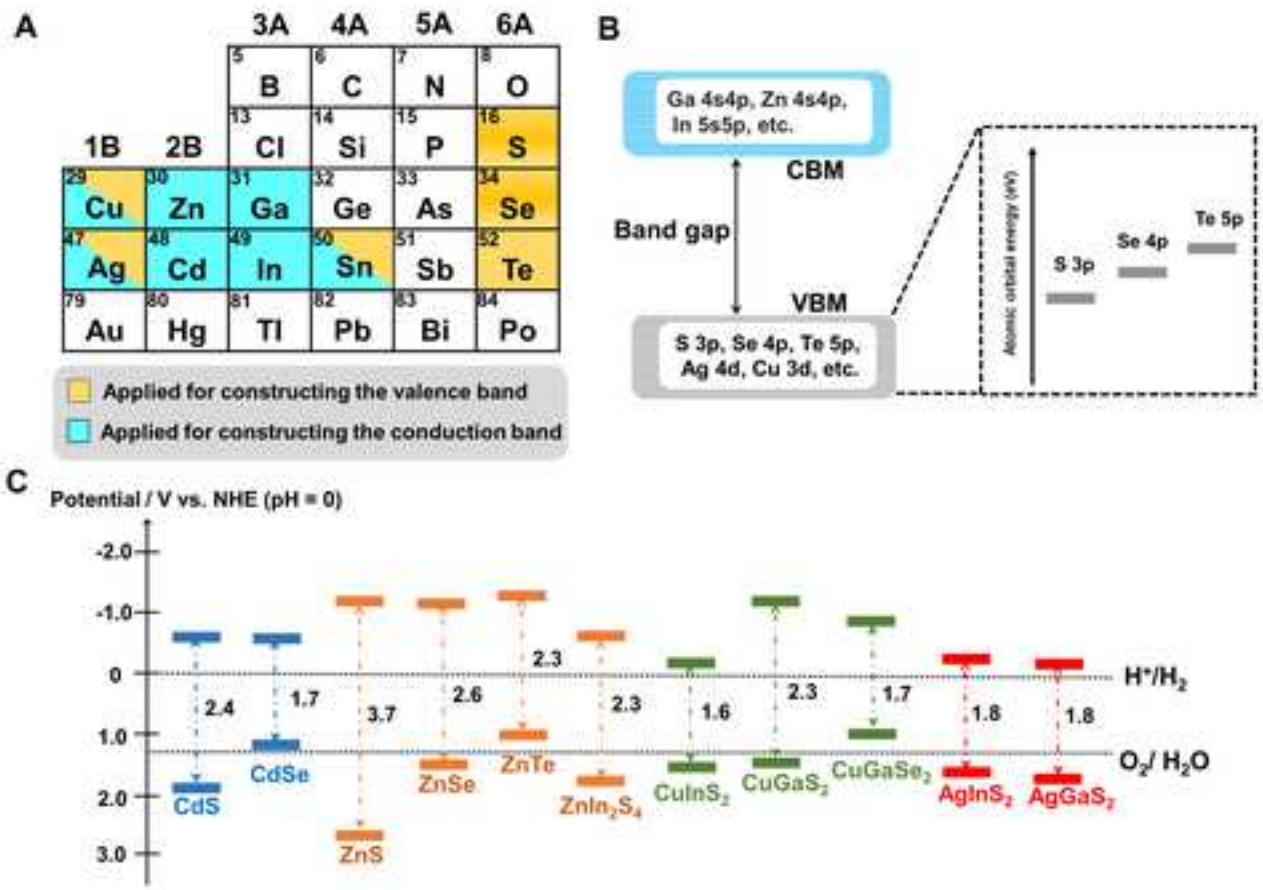

Figure 3

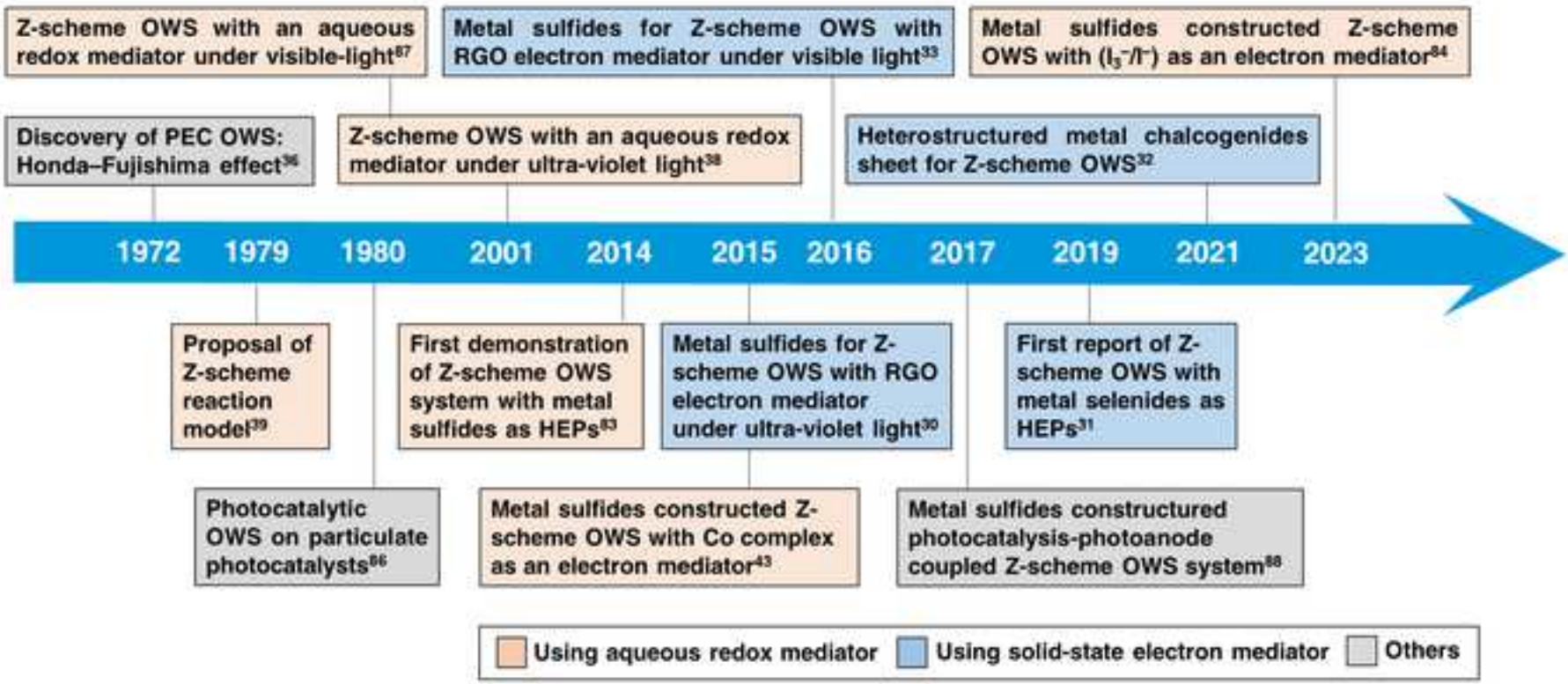

Figure 4

Click here to access/download;Figure;Figure 4.TIF

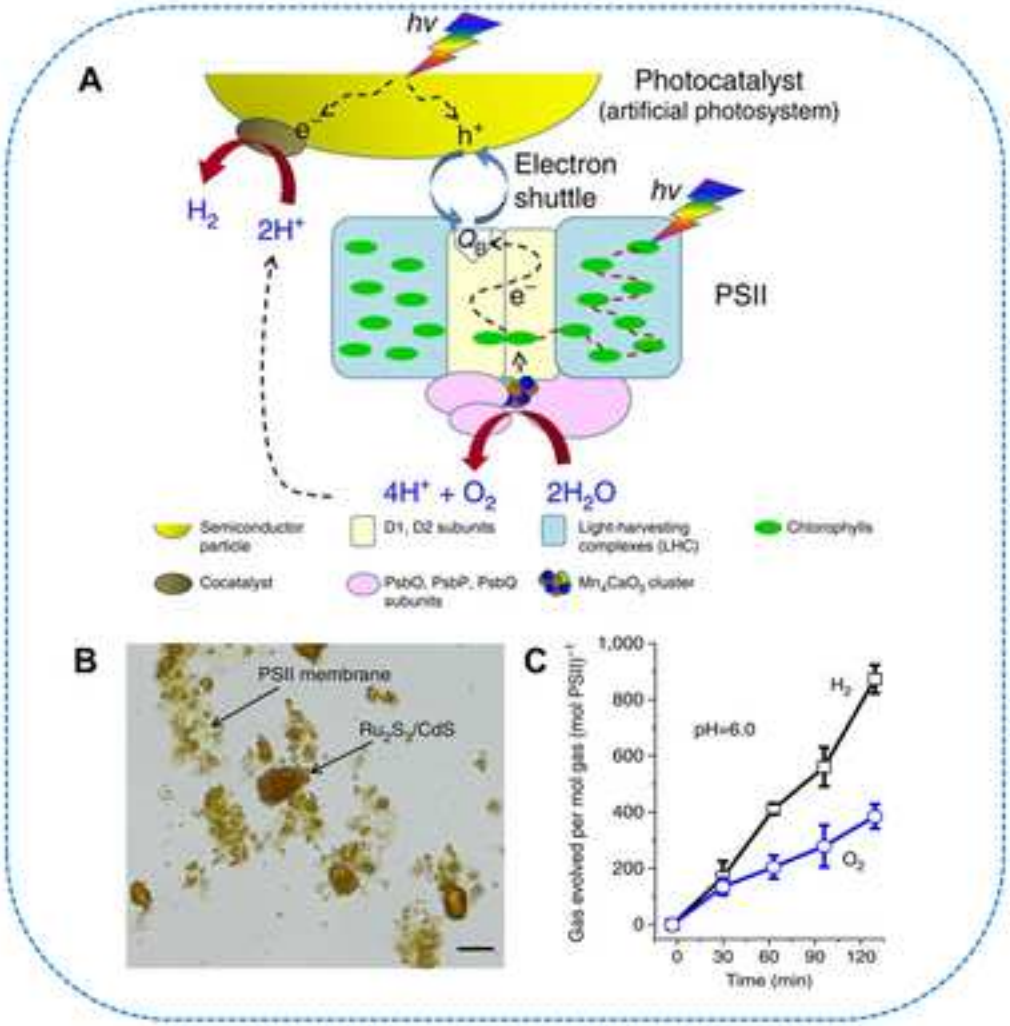

Figure 5

Click here to access/download;Figure;Figure 5.TIF

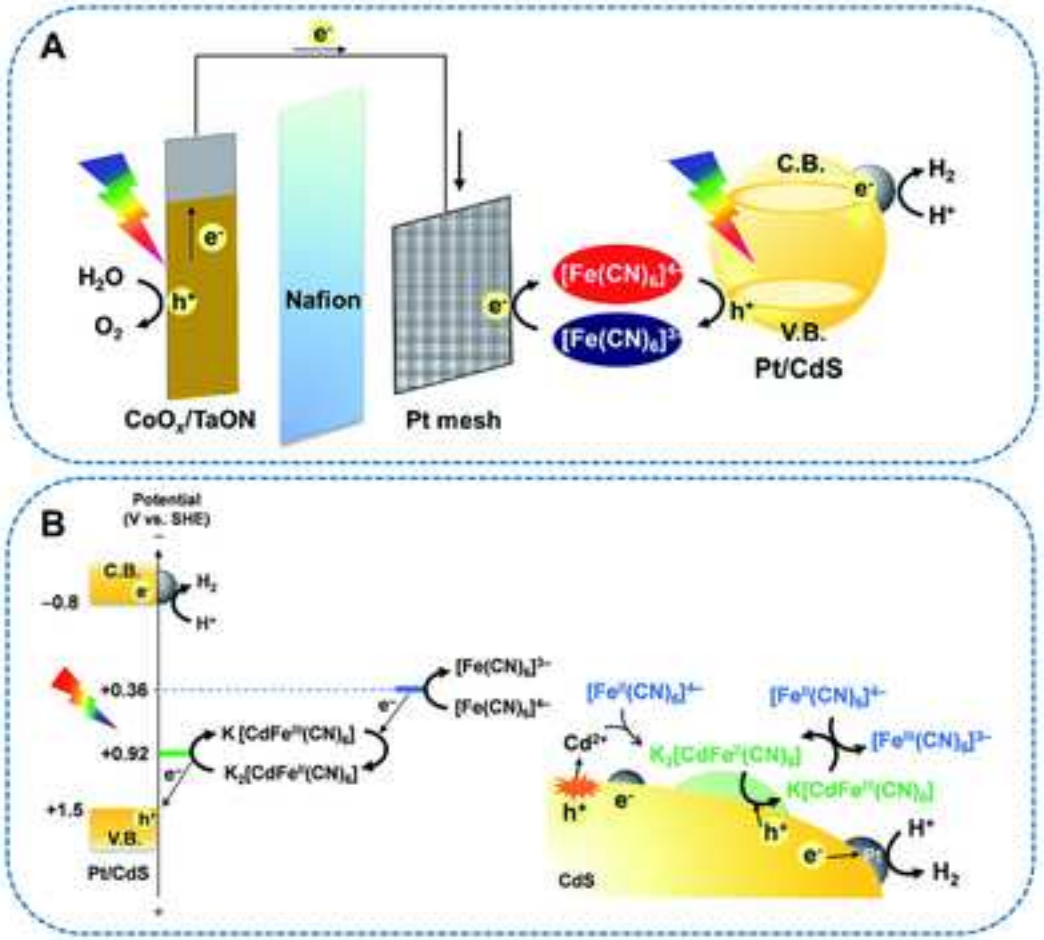

Figure 6

Click here to access/download;Figure;Figure 6.TIF

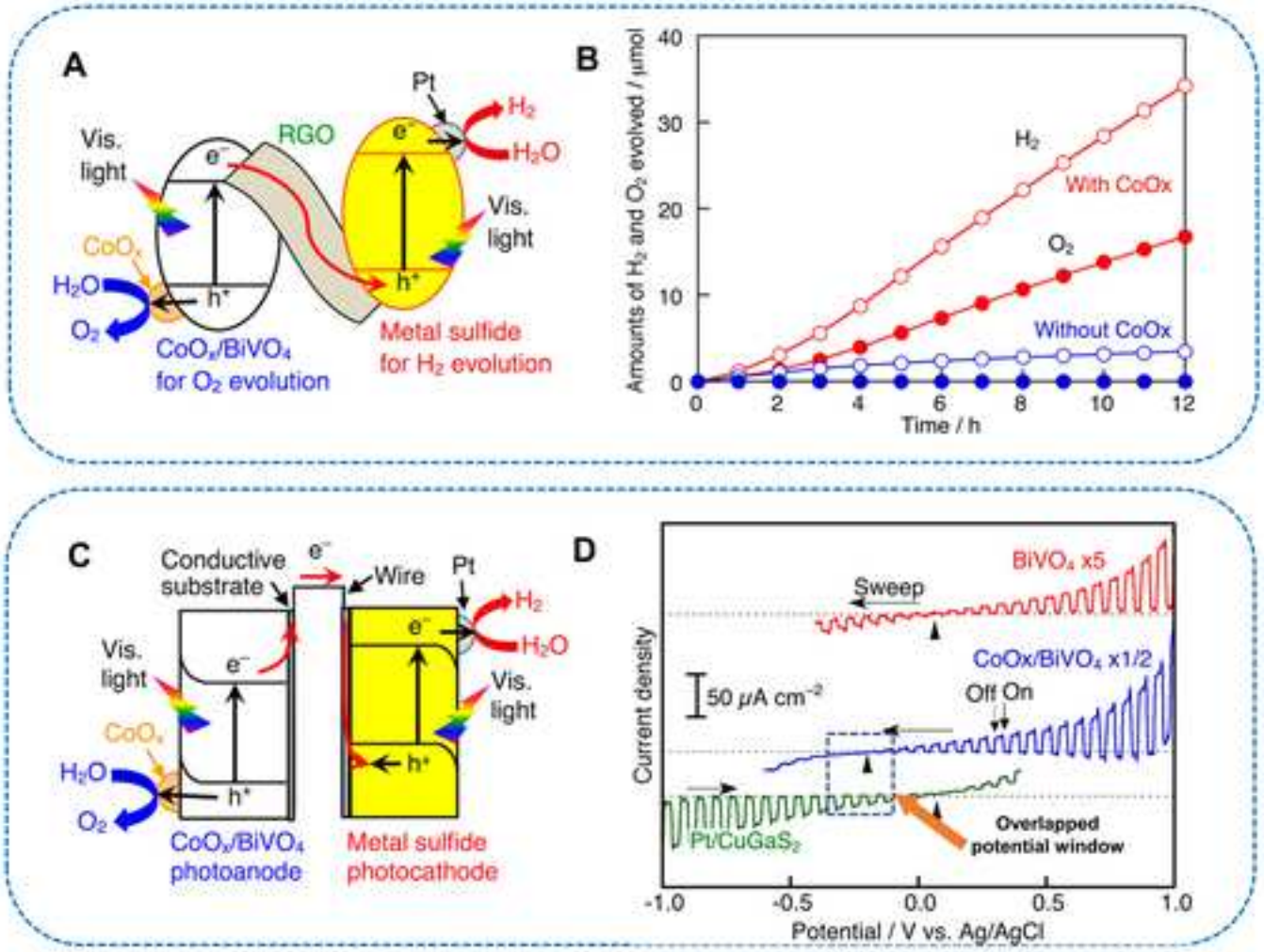

Figure 7

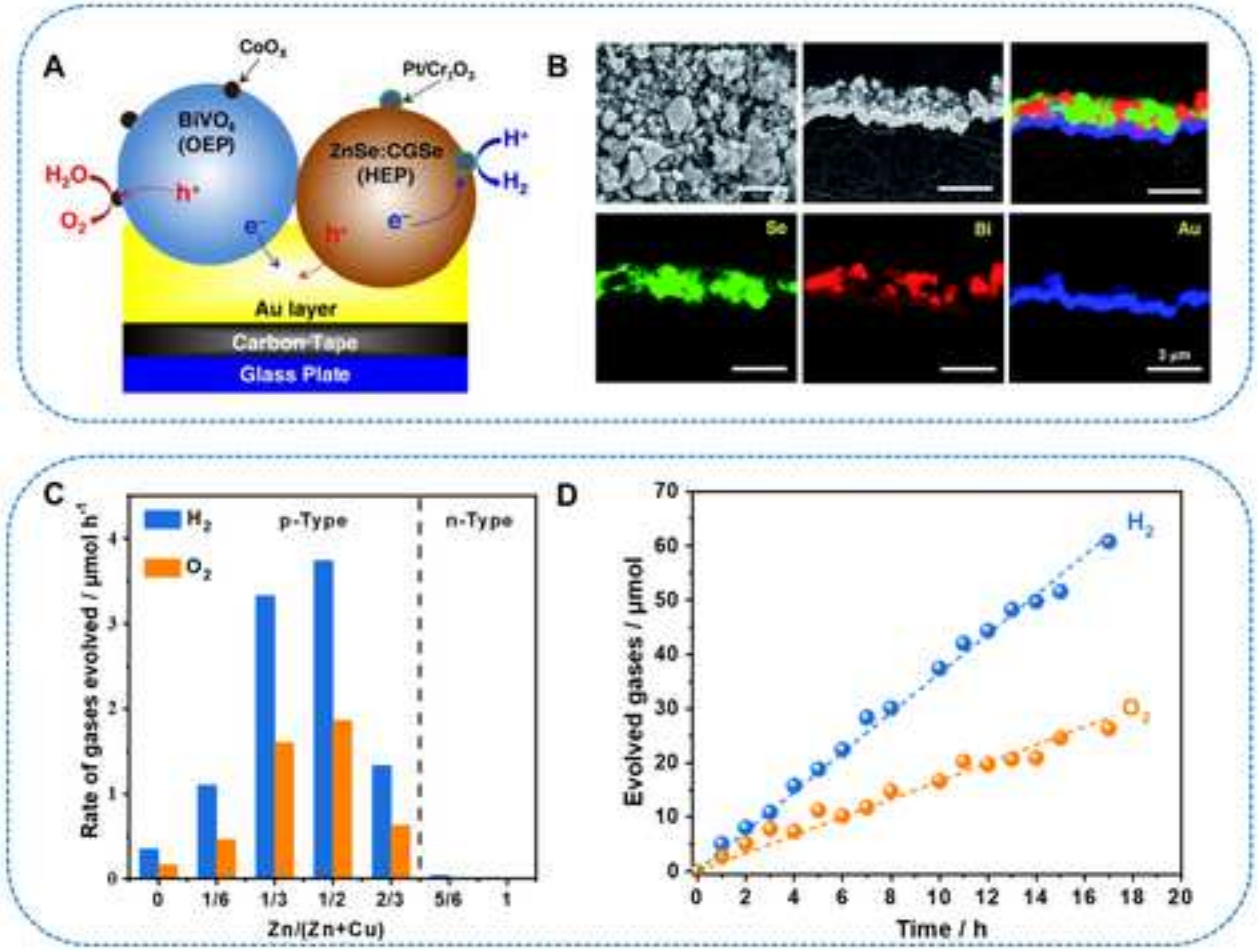

Figure 8

Click here to access/download;Figure;Figure 8.TIF

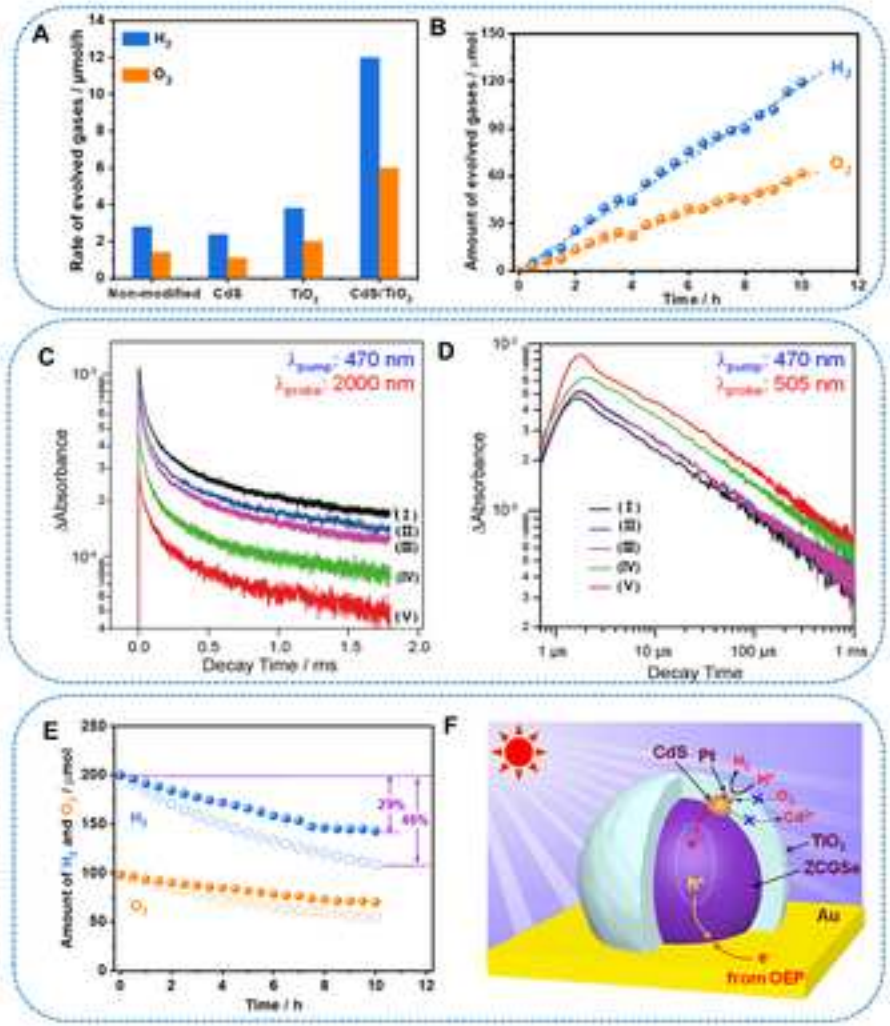

Figure 9

Click here to access/download;Figure;Figure 9.TIF

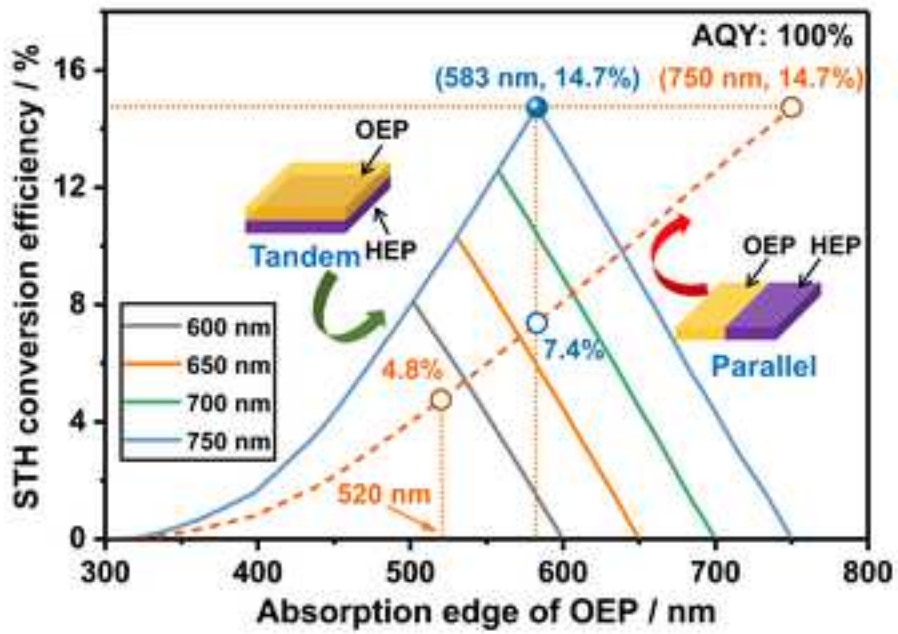

TOC